Radiographic Imaging in Implant Dentistry

10

Andreas Stavropoulos, Kristina Bertl, Florian Beck, Paolo Cattaneo, and Ann Wenzel

10.1 Introduction

Radiographic imaging is key in all phases of dental implant therapy, i.e., diagnosis, planning and assessment of treatment, and long-term monitoring, both in terms of clinical practice and in implant research. Traditionally two-dimensional (2-D) imaging has been the standard in clinical practice and research; however, recent technological advances and increased access to new technologies have made three-dimensional (3-D) imaging quite common in both clinical practice and research (e.g., cone-beam computed tomography; CBCT). Considering potential health risks due to radiation exposure, it is important to understand the possibilities and the limitations of the various radiographic techniques and technologies to assess the recipient bone for implant planning and the bone-to-implant interface and peri-implant bone level after installation.

10.2 Periapical Radiographs

Periapical radiographs can be used for treatment planning in straightforward cases, but they are most commonly used for assessing the marginal peri-implant bone levels at follow-up. Evaluation of the marginal peri-implant bone level, i.e., the distance from the most coronal bone crest to a specific implant landmark—commonly the margin of the implant collar—is relevant in implant research when assessing the effect of various implant macro-designs and surface technologies on the physiological bone remodeling occurring after implant installation and loading, or when assessing various surgical techniques, as the goal is to have the entire implant body within the bone. Further, monitoring the marginal peri-implant bone level and assessing possible

A. Stavropoulos (✉)
Department of Periodontology, Faculty of Odontology, Malmö University, Malmö, Sweden

Division of Conservative Dentistry and Periodontology, University Clinic of Dentistry, Medical University of Vienna, Vienna, Austria
e-mail: andreas.stavropoulos@mau.se

K. Bertl
Department of Periodontology, Faculty of Odontology, Malmö University, Malmö, Sweden

Division of Oral Surgery, University Clinic of Dentistry, Medical University of Vienna, Vienna, Austria

Department of Periodontology, Dental Clinic, Faculty of Medicine, Sigmund Freud University, Vienna, Austria

F. Beck
Division of Oral Surgery, University Clinic of Dentistry, Medical University of Vienna, Vienna, Austria

P. Cattaneo
Division of Orthodontics, Department of Dentistry and Oral Health, Aarhus University, Aarhus, Denmark

Melbourne Dental School, Faculty of Medicine, Dentistry and Health Sciences, Melbourne, Australia

A. Wenzel
Division of Oral Radiology, Department of Dentistry and Oral Health, Aarhus University, Aarhus, Denmark

changes (i.e., bone loss) between different time points is essential, as stability of the marginal peri-implant bone level is considered the most reliable sign of peri-implant health [1]. In this context, various cut-off values of bone level have been suggested and employed among studies and classification systems to discriminate between a healthy implant and an implant with peri-implantitis [2, 3]. Nevertheless, it is accepted that there is some variation in crestal bone level distances that is compatible with peri-implant health. This variation depends, among other factors, on the implant system, i.e., different implant systems experience a different amount of crestal bone loss due to initial bone remodeling after implant installation and/or loading. It is thus obvious, that dimensional accuracy of the depicted/registered anatomical structures around implants is very important.

10.2.1 Distortion

Periapical radiographs of good quality provide high spatial and contrast resolution and thus sharp images but may show some degree of image magnification depending on the relative focal spot-to-film and object-to-film distance [4]. In general, an average magnification of 5% is usually accepted for periapical radiographs recorded with the paralleling technique [5], irrespective of the site within the mouth. Nevertheless, studies comparing measurements/distances of structures recorded in periapical radiographs with direct measurements showed that the range of differences may be quite large. For example, Sonick et al. [6] compared the localization of the mandibular canal with the clinically measured distances and those made in periapical images obtained by a long-cone paralleling technique, with a film holder attached to the tube of the X-ray unit; the difference in absolute values between clinical and radiographical measurements was only 1.9 mm on average, however, a range of 0.5 to 5.5 mm was observed, which in turn translated into a magnification ranging from 8% to 24% (14% on average). Similarly, Schropp

et al. [7] observed an average magnification of 6% when evaluating the distortion of metal calibration balls recorded in periapical radiographs, however, the range was from 1% to 12%. Although the dimensional distortion in periapical radiographs may not constitute a major problem in everyday clinical work, estimation of the true magnification is necessary for studies on the prevalence of peri-implant biological complications and differential diagnosis (i.e., mucositis and peri-implantitis), and/or for early detection of peri-implantitis to allow timely therapeutic interventions. Indeed, studies assessing the prevalence and/or incidence of peri-implantitis require not only the presence of clinical signs of disease but also the presence of bone loss beyond the crestal bone level changes resulting from initial bone remodeling, taking also a measurement error in periapical radiographs of 0.5 mm, on average, into account [8]. In this context, estimation of the true magnification in periapical radiographs appears imperative for research purposes.

Several methods have been suggested for calibration purposes of periapical images, for example, the use of cylindrical metal markers [9] or of a metal ball with a standardized diameter [7] (Fig. 10.1). Autoclavable cylinder metal markers, used often as indicators for implant angulation during treatment planning, can also be used for calibration purposes. However, despite the fact that no information on the implant angulation can be obtained by means of a metal ball, this method offers the advantage that projection geometry does not influence the radiographic image due to the symmetrical shape of the ball, and thus, is to be preferred. In context, in periapical images depicting implants, it is most often not necessary to include a reference marker, since the implant itself can be used for calibration purposes, provided that information on implant dimensions is retrievable or the distance between the peaks of the implant threads is known. Obviously, using the peaks of the implant threads for calibration purposes requires that radiographs show an optimal projection geometry in the vertical plane, i.e., the image displays sharp threads with no overlaps on both sides of the implant.
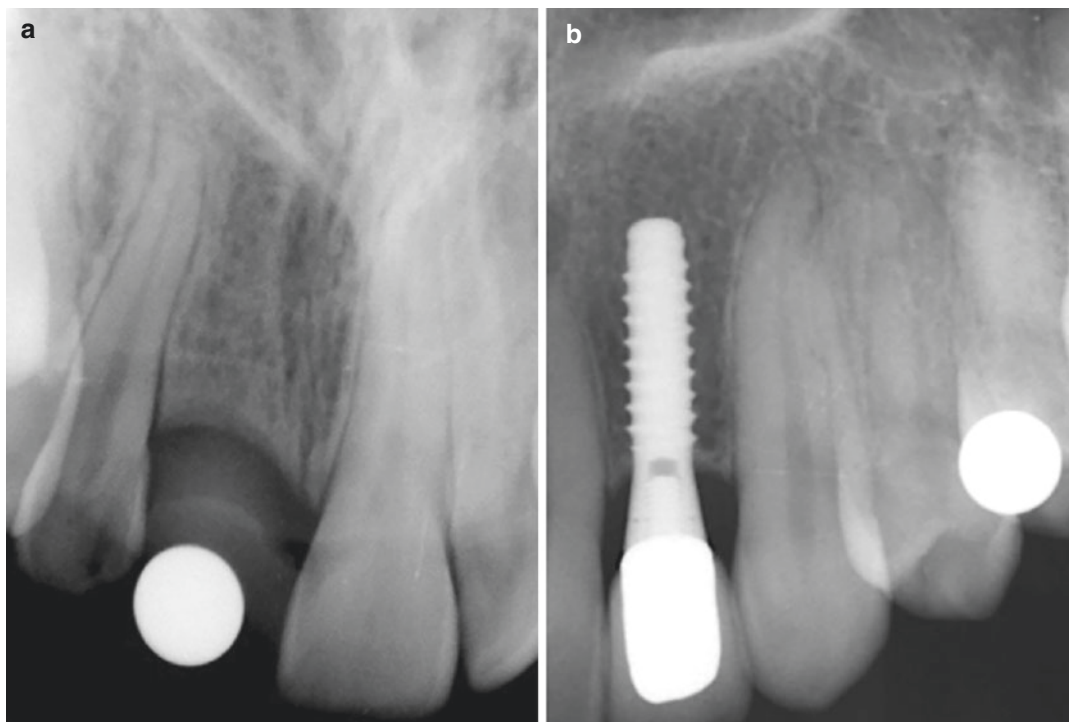
Fig. 10.1 A metal ball (5 mm diameter) can be used for calibration purposes in periapical radiographs, during treatment planning where no implant is included (**a**), but also when an implant of unknown dimensions is registered (**b**)

Nevertheless, in cases where pre-surgical radiographs (i.e., without an implant) are included in the analysis, a metal ball or other reference marker should be used.

10.2.2 Projection Geometry

Proper projection geometry in the vertical plane, so that the implant displays sharp threads with no overlaps on both sides, is important not only for calibration purposes but also to facilitate proper assessment of the marginal peri-implant bone level at follow-ups. For example, in a radiograph taken with the radiation beam being not perpendicular to the long axis of the implant, the threads of a screw-type implant appear blurred on either side of the implant; this may not allow for properly define the most coronal bone-to-implant contact (BIC). On the other hand, with an optimal projection angle in the vertical plane, i.e., the

film/digital receptor is positioned parallel to the implant axis, and the radiation beam is directed perpendicular to this axis, the implant image displays sharp threads with no overlaps on either side allowing proper evaluation and recording of the peri-implant bone levels (Fig. 10.2).

Proper projection geometry in periapical radiographs is also crucial for controlling for possible risk factors for technical or biological complications, e.g., the misfit between implant and/or prosthetic components, component fracture, or cement remnants (Fig. 10.3). Obtaining implant images with optimal projection geometry may be challenging due to the fact that implants are often not inserted with an inclination corresponding to that of the alveolar process or neighboring teeth. This might especially be the case in fully edentulous patients, but also in single tooth gaps in agenesis sites where variable amounts of alveolar bone may be missing. Thus, correct alignment of the radiation beam is often difficult
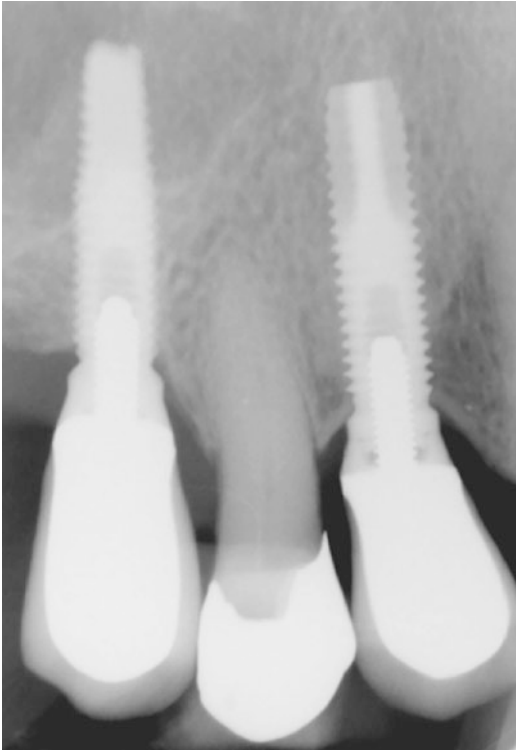
Fig. 10.2 The left implant image presents with threads blurred on either side, which makes it difficult or impossible to properly define the most coronal radiographic BIC. In contrast, the right implant presents with sharp threads and no overlaps on either side of the implant, making identification of the most coronal radiographic BIC easy. Due to differences in the implant inclination within the jaw, the radiation beam was not perpendicular to the long axis of the implant and the sensor for the left implant, but it was for the right one

to predict when the implant is still submerged or before the prosthetic restoration has been mounted; but even in cases including the prosthetic restoration, correct determination of the implant axis by clinical examination might be impaired as the abutment and restoration may be angulated.

Depending on the direction of the radiation beam, i.e., the beam has either an obtuse or an acute angle in relation to the long axis of the implant, the implant threads of a screw-type implant appear on the radiograph mostly blurred on the left or right side, respectively [10]; this is irrespective of whether the implant is placed in the upper or lower jaw. In the case of radiographs

with blurred implant threads, the "RB-RB/LB-LB" mnemonic rule, suggested by Schropp et al. [11], can be applied in order to correct the inclination of the X-ray tube and obtain a second image with sharp implant threads. RB/RB means, "if Right Blur, then Raise Beam" (Fig. 10.4), i.e., if the threads are mostly blurred at the right side of the implant image, the X-ray beam direction must be raised towards the ceiling to obtain sharper threads on both sides. Accordingly, LB/LB means, "if Left Blur, then Lower Beam," i.e., if the implant threads are mostly blurred at the left side of the implant image, the X-ray beam direction must be lowered towards the floor to obtain sharper threads on both sides.

The degree of beam correction needed can be roughly estimated by the degree of implant thread overlapping; i.e., if the threads on one side of the implant image are still rather clearly discernible, a correction of the radiation beam of up to about 10° is needed, while if the threads in both sides of the implant image are poorly discernible, a correction of the radiation beam of about 20° is needed (Fig. 10.5) [12]. Obviously, a prerequisite for the RB-RB/LB-LB mnemonic rule to properly function is that the film/sensor is also repositioned so that the radiation beam is kept perpendicular to the film/sensor, e.g., by means of a holder, while the position of patient's head remains stable during the repeated exposures.

Implementation of the RB-RB/LB-LB mnemonic rule has been proven rather easy, since even operators inexperienced in radiography (third-year dental students), after a short instruction in the use of the rule, were able to record higher quality implant images in 2/3 of the cases by changing the vertical projection angle in the correct direction from one exposure to the next [11]. Specifically, in this in vitro study, after an average of only 2 exposures, images either perfectly sharp or only with slightly blurred threads, were obtained, even in cases of extreme—compared to the neighboring teeth—implant inclinations. In another in vitro study, after a maximum of 2 exposures, no significant differences were observed between the use of the RB-RB/LB-LB mnemonic rule or the use of customized rigid imaging guides (acrylic splints) in terms of effi-
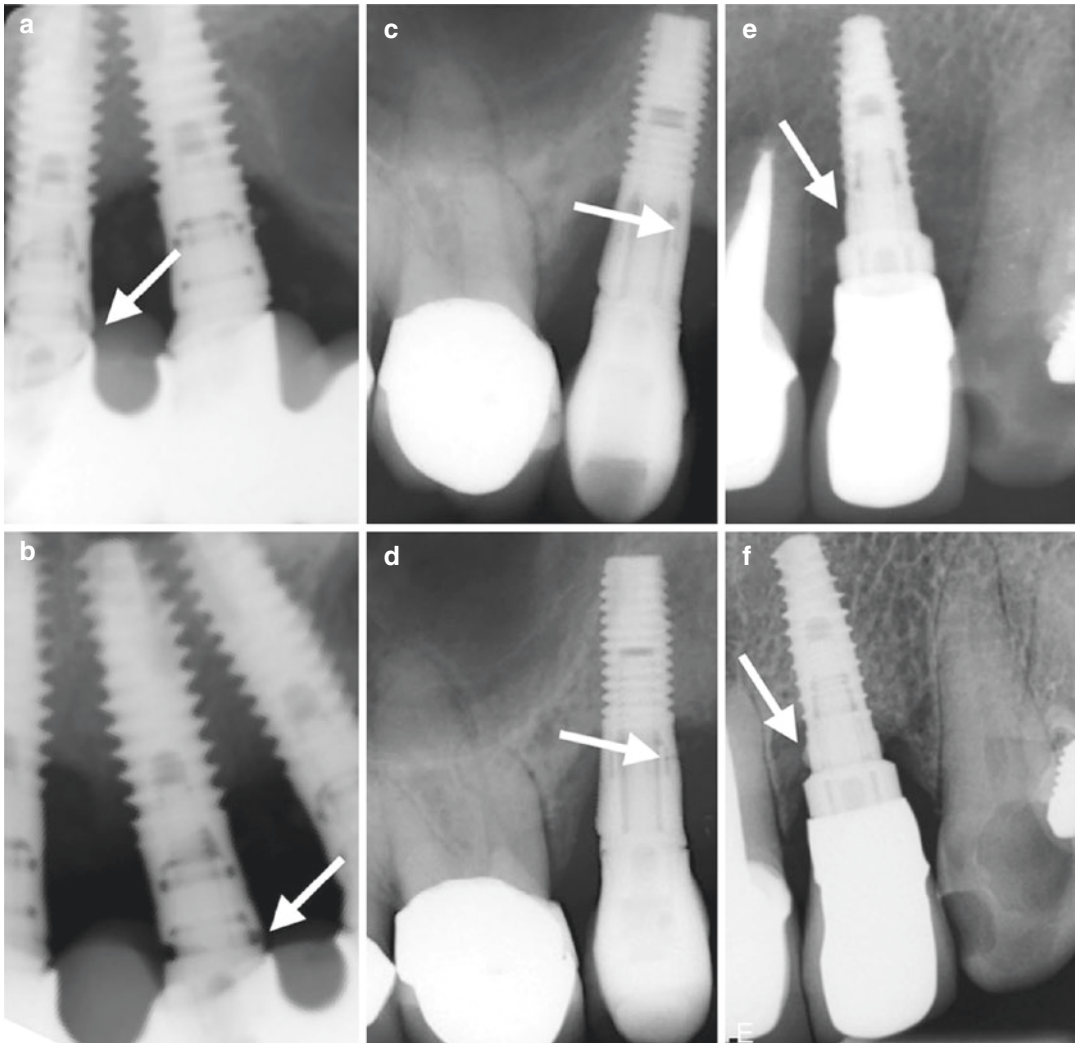
Fig. 10.3 Examples of radiographs with improper (**a**, **c**, **e**) and proper (**b**, **d**, **f**) projection geometry. Proper projection geometry, i.e., the radiograph is taken with the radiation beam being perpendicular to the long axis of the implant, facilitates proper diagnosis of technical and biological complications, e.g., misfit of prosthetic components (**a** vs. **b**), fracture of the implant neck (**c** vs. **d**), and cement remnants (**e** vs. **f**)

cacy of obtaining images with perfectly sharp threads or images with only slightly blurred threads, i.e., more than 70% of the cases were judged acceptable or perfect [13]. In perspective, considering the relatively limited added benefit and the much larger effort needed for constructing a customized imaging guide, it is reasonable to suggest that for monitoring purposes in the clinic or in large field studies the RB-RB/LB-LB mnemonic rule is sufficient.

10.2.3 Reliability of Measurements

For standard monitoring of implants in the clinic, a crude method of evaluating the stability of peri-implant bone levels in consecutive periapical radiographs is by simply comparing the level of marginal peri-implant bone to a reference landmark; for example, counting the number of implant threads with no BIC in radiographs taken at different time points is an easy way to assess
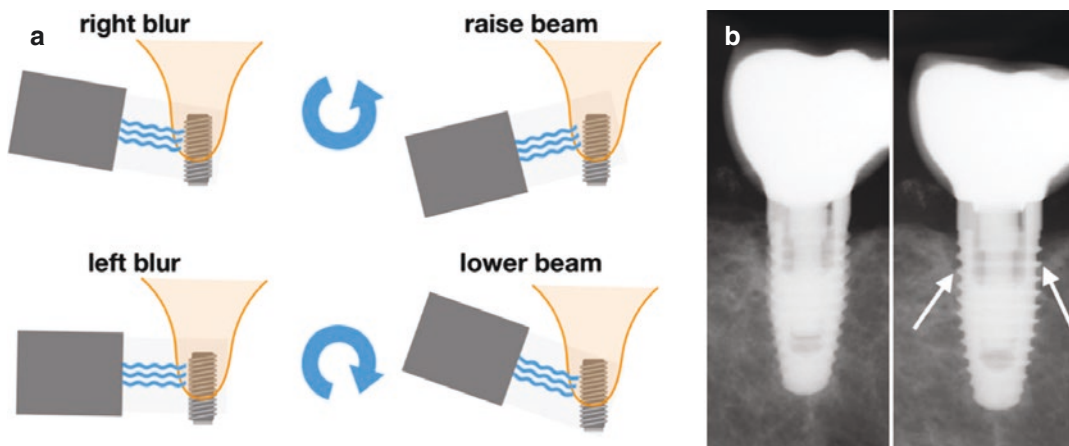
Fig. 10.4 Graphic presentation of the RB-RB/LB-LB mnemonic rule (**a**), with an implant inserted in the upper jaw. If the implant threads are mostly blurred at the right side of the implant image, the radiation beam direction must be raised towards the ceiling to obtain sharper threads on both implant sides. If the implant threads are mostly blurred at the left side of the implant image, the radiation beam direction must be lowered towards the floor to obtain sharper threads on both implant sides. (**b**) An implant in position 45 is registered with blurred threads, mostly at its left side; to the right, a new exposure with the beam lowered by about 15° results in an implant image with sharp threads at both sides allowing identification of the radiographic BIC. It is noteworthy that the RB-RB/LB-LB mnemonic rule applies irrespective of whether the implant is placed in the upper or lower jaw

Fig. 10.5 For screw-type (threaded) implants, a deviation of the radiation beam of up to about 10° from the right angle to the axis of the implant, results in an implant image with threads at either side still rather clearly discernible (right implant); when the deviation of the radiation beam is about 20° or more, the threads are poorly discernible at both sides of the implant image (left implant)

progressive bone loss. For research purposes, however, where high data precision is mandatory, peri-implant bone levels may be evaluated by measuring the distance from a reference landmark to the most coronal radiographic BIC by means of image analysis software. Usually, the shoulder of the implant is used as the fixed reference landmark, as it most often corresponds to the level of the bone at insertion (for bone-level implants) and is generally readily recognizable (Fig. 10.6).

Depending on the type of implant connection and/or abutment or prosthetic material type, identification of the fixture-abutment margin can be sometimes difficult; in such cases the margin of the prosthetic restoration or the apex of the implant can be used as a fixed landmark (Fig. 10.7). However, in such cases, only relative changes in bone levels (e.g., between two time points) should be considered, as the level of the bone at insertion cannot be determined.

In this context, the accuracy of radiographic recordings of marginal bone levels in terms of representing the true (histological) marginal peri-implant bone levels has been assessed in pre-clinical in vivo studies using clinical-type implants. Most of the studies showed that radiography underestimates peri-implant bone level
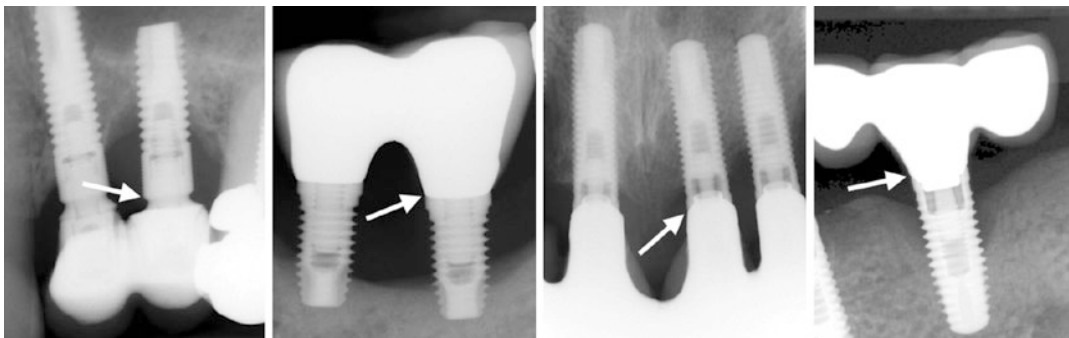
Fig. 10.6 The implant shoulder (indicated by the arrows) is usually quite easily identified and is commonly used as the reference landmark because it most often corresponds to the level of the bone at insertion (for bone-level implants)
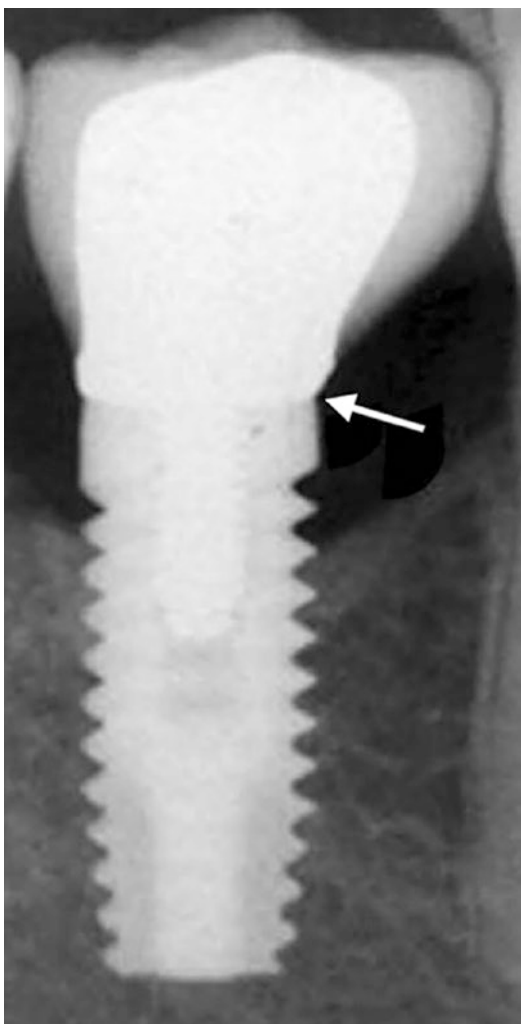

Fig. 10.7 When the implant shoulder cannot be identified, the margin of the prosthetic restoration (arrow) or the apex of the implant can be used as the fixed landmark for assessing relative changes in bone levels

in the majority of cases with about 0.5 mm [14–18]. For example, one study in dogs showed a correlation of 0.7 ($p < 0.01$) between bone level measurements made in digital intraoral radiographs and in histological sections, while the differences were 0.5 mm or less in half of the cases, but the average difference between radiographic and histological measurements was 1.17 mm. Similarly, another study showed that the radiographic evaluation underestimated the bone level by 0.6–1.4 mm [17, 18]. These observations imply that radiography may indeed in some cases fail in diagnosing a considerable amount of bone loss. In perspective, it has been demonstrated that probing pocket depth measurements (with or without standardized probing force) at implant sites do not necessarily correlate well with the bone level either. Specifically, depending on the degree of inflammation in the peri-implant tissues, the probe tip is farther from or closer to the bone level (in healthy and in inflamed tissues, respectively) [19, 20], and additionally, the prosthetic reconstruction often interferes with proper probe positioning/angulation [21] (Fig. 10.8).

Thus, the marginal peri-implant bone level can be estimated more precisely in periapical radiographs than with clinical probing, while no significant differences have been reported between conventional and digital periapical radiography (i.e., sensors or photostimulable phosphor plate systems) regarding the diagnostic accuracy in detecting and estimating the size of peri-implant defects [22–26]. It is however important to keep in mind that radiographic evi-
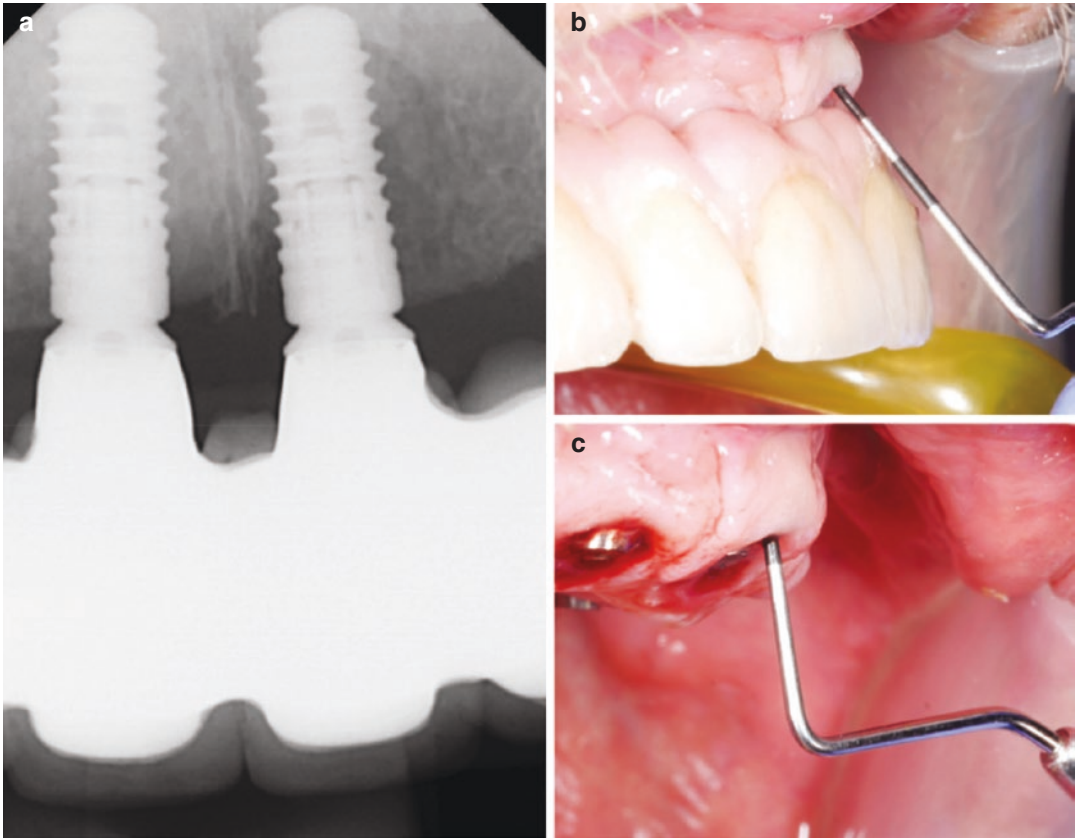
Fig. 10.8 The implant in position 21 has completely lost osseointegration (**a**) and harbors a very deep pocket which cannot be properly probed (**b**) due to the configuration of the prosthetic reconstruction interfering with a proper probe angulation (**c**)

dence of BIC does not necessarily imply osseointegration on the histological level [27].

A limitation of periapical images is that they display only a limited part of the alveolar process and consequently may in some instances register only part of an implant; e.g., in situations where extensive bone loss due to disease and/or physiological remodeling after long periods of edentulism has resulted in the implant placed "too deep" in comparison with the neighboring alveolar crest (Fig. 10.9) or cases with a flat palate impeding proper placement of the sensor (Fig. 10.10). In most cases, this poses no problem, as it is more important to display the coronal part of the implant with sharp threads for optimal bone level estimation than to image the apical part of the implant.
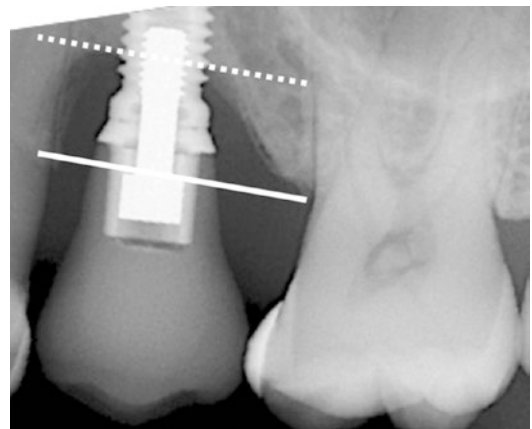

Fig. 10.9 The implant in position 25 is placed "too deep" in comparison with the neighboring alveolar crest and thus, it is difficult to register the entire implant length with proper projection geometry

Fig. 10.10 In the case of a flat palate (**a**), proper placement of the film holder/sensor is not possible (**b**), resulting in recording only a part of the implant (**c**); in this particular case, the peri-implant bone level is at the normal level for this specific type of implant, hence not displaying the entire implant does not pose a diagnostic problem

10.3 Panoramic Radiographs

Panoramic radiography provides an overview of the jaws and the overall status of the teeth and surrounding periodontal and periapical conditions, including the interrelations of the various neighboring anatomical structures. Panoramic radiographs are cheap and highly available, and the radiation dose of digital equipment is comparable to approximately 4 periapical radiographs. On the other hand, due to the projection technique panoramic radiographs also display an overlap of non-dental anatomic structures (e.g., the spine) or among neighboring teeth (particularly among the premolars in the upper jaw). Additionally, the lower spatial resolution and the enlargement factor must be considered; such issues may negatively influence measurement precision and accuracy.

In studies evaluating the periodontal bone level in panoramic or periapical images in comparison with direct intra-surgical measurements, panoramic images had a significantly lower accuracy than periapical images in terms of detecting bone loss and estimating the bone level (i.e., mostly underestimating the bone level) [4, 27, 28]. Thus, up-to-now panoramic radiography cannot be considered the method of choice for research purposes for evaluating details regarding the outcome of treatment or for monitoring the peri-implant bone level as measuring precision is required. Panoramic examination has been used, however, for evaluating the outcome of maxillary sinus augmentation procedures, because the entire sinus including the apical portion of the implant can be more easily visualized in these images compared to the smaller-field periapical radiography [29, 30]. In general, a panoramic image is often used when more than one implant are to be installed, for selecting the appropriate implant size and position during treatment planning in straightforward cases where the bucco-lingual dimension of the alveolar process can be clinically judged. Nevertheless, the distortion and enlargement of structures in the image have to be taken into consideration by a calibration procedure.

Panoramic images are not considered appropriate for evaluating marginal peri-implant bone conditions in the clinic, although, in specific clinical situations, panoramic radiographs may be preferred to periapical radiographs. For example, in cases with many implants, where proper radiographic registration of implants is cumbersome or even not possible with periapical radiography due to the anatomical situation; e.g., in cases of highly atrophied mandibles, where the residual alveolar process is close to or at the level of the floor of the mouth. In this context, it has to be noted that the image quality, including the frontal regions, has substantially improved during recent years due to technically controlled, more penetrating radiation given to this region during the exposure that blurs the shadow of the spine in the image (Fig. 10.11). Further, new-generation radiographic devices allow for registering segmented panoramic images in the vertical or horizontal plane, which de facto reduces the radiation
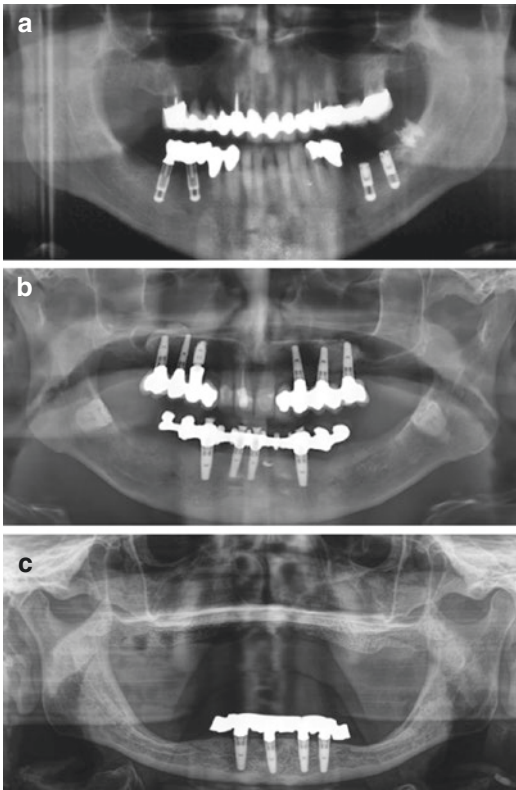
Fig. 10.11 The evolvement of the quality of panoramic radiographs from analog (**a**) to different generations of digital images (**b**, **c**)

burden to the patient and often results in sharper images. Thus, the usefulness of panoramic radiography may increase in the future.

10.3.1 Distortion

In general, a rather large magnification is inherent in panoramic images and depends on several factors, such as patient position/malposition, mandibular angulation, and equipment [31–34].

Magnification moreover varies among the regions of the mouth in the same image, as well as in the horizontal and vertical plane. In a clinical study involving patients to receive implants in various regions of the mouth [7], the true magnification in panoramic images was estimated by measuring the dimensions of a standardized metal ball of known size that was placed close to the anticipated implant site during exposure; although the average magnification was 22%, a great variation in magnification existed, ranging from −10 to 90%. Furthermore, it was observed that a larger variation in magnification was found in the horizontal plane than in the vertical plane (i.e., distortion), and the largest deviation from the standard magnification factor of 25% was seen in the horizontal plane and was most pronounced in the maxillary anterior region [7]. Furthermore, in another ex vivo evaluation (unpublished data), 25 metal balls 5 mm in diameter were placed buccally at the height of the crown and of the apex in the upper and lower jaw of a dry human skull, and at the occlusal plane in the molar, premolar, and anterior region (Fig. 10.12); the images of the spheres presented often as an ellipse with different orientation and magnification depending on the position of the sphere, with the maximum and minimum diameter of these ellipses ranging between 4.58–5.85 mm and 3.11–5.03 mm, respectively. In perspective, based on the fact that large variation in panoramic image distortion exists, depending on the region in the mouth as well as on the equipment, it seems reasonable to suggest that for research purposes a reference marker of known dimensions, like the metal ball mentioned before, should be placed on top of the alveolar process in the area of interest during exposure and used for calibration to true size measurements [35].
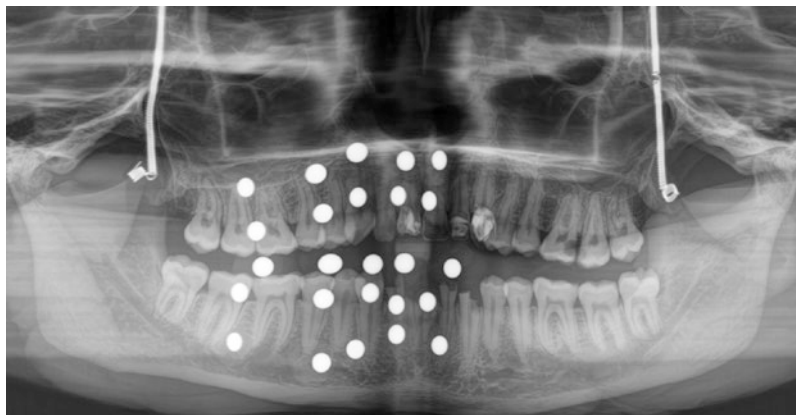
Fig. 10.12 Panoramic radiograph of a dry human skull with 25 metal balls (each 5 mm in diameter) placed buccally at the height of the crown and apex in the upper and lower jaw, and at the occlusal plane in the molar, premolar, and anterior region. Depending on the region, the metal balls were displayed as ellipses in different orientations and magnifications with up to almost 1 and 2 mm differences from the actual diameter of 5 mm if the maximum and minimum diameter, respectively, was measured

10.4   3-D Radiography

10.4.1 CBCT

An obvious disadvantage of both periapical and panoramic radiography is that a 2-D image of 3-D structures is displayed. The missing buccolingual dimension can be captured with cross-sectional radiography, such as conventional computed tomography (CT) or CBCT. All 3-D radiographic techniques have in most studies been found superior to intraoral and panoramic radiography in visualizing anatomical structures, e.g., the mandibular canal [6, 36–44]. 3-D radiographic techniques (i.e., CT and CBCT) have also been found superior to periapical radiography in identifying various types of artificially created bone defects (including periapical defects) [45–49] or bone lesions of endodontic origin [50, 51]. In a study comparing the image quality and visibility of anatomical structures in the mandible among five CBCT scanners and one multi-slice CT system (MSCT), CBCT was found to be comparable or even superior to MSCT [52]. CT and CBCT offer also the advantage, compared with periapical and panoramic images, of practically no dimensional distortion, as well as the possibility of visualizing 3-D reconstructions of the registered hard tissues. Due to the considerably lower radiation dose of CBCT compared to CT, the constantly increasing quality, smaller fields-of-view, and lately affordable prices, CBCT is a prevailing technology [53].

CBCT may be used in implant dentistry for implant treatment planning, for example, in cases where clinical examination or conventional radiographic techniques may indicate inadequate bone volume for implant installation or anatomical aberrations are suspected that may require special attention or modification of the surgical technique, e.g., a narrow residual alveolar ridge or a deep submandibular fossa, or the presence of septa when a sinus lift augmentation procedure is planned [54]. In this context, studies have assessed how the additional information from the third dimension, i.e., the bucco-oral bone width, changes the selection of the implant size when compared with planning based on information from a panoramic image [55–58]. For example, in one study involving 121 single implant sites, the implant size selected based on only panoramic images differed in almost 90% of the cases in width and/or length from that selected with CBCT, having access to additional information on the bucco-oral width [58]. Further, approximately

50% of the anterior implants planned based on information from CBCT were narrower compared to those planned based on a panoramic radiograph. Similarly, in another study on 71 patients with 103 implant sites, planning based on CBCT re-categorized the majority of cases into a narrower or shorter implant size compared with planning based solely on panoramic radiographs [55]. With regard to sinus lift, although in most cases a panoramic radiograph is considered sufficient for planning a sinus augmentation procedure, a preoperative CBCT scan increased surgical confidence and detection rate of sinus septa and mucosal hypertrophy [59–61]. In fact, a study involving 101 patients judged in need of a sinus lift procedure based on periapical and/or panoramic radiographs showed that in about 65% of the cases, an implant of at least 8 mm could be placed without sinus augmentation when planning was based on CBCT [62]. Indeed, a recent study demonstrated that due to the high variability of the dimensions of the maxillary sinus, both in-between patients but also in-between tooth regions within the same patient, the bucco-oral sinus width cannot be assumed based on the residual bone height or standard values [63]. Thus, although there is no evidence that implant treatment planning or sinus lift procedures based on a CBCT examination result in better treatment results than those based on panoramic images, one may consider that knowing the proper implant size prior to surgery may be advantageous for the surgeon in order to be as well prepared as possible (e.g., alternative implant sizes in stock, instrumentation and material necessary for additional procedures like lateral bone augmentation, etc.), and of course for the patient in case that a more invasive procedure can be avoided.

Except treatment planning, CBCT has been used for the diagnosis of symptoms of unclear etiology associated with implants (e.g., paresthesia) (Fig. 10.13) and/or of bone defects associ-

Fig. 10.13 The paresthesia reported by the patient since the time of implant placement could not be explained based on the information provided by the panoramic radiograph (**a**), but was easy to explain with the bucco-oral section provided by the CBCT (**b**); the implant apex is violat- ing the coronal/lingual aspect of the mandibular canal (arrow)

ated with implants, for assessing the marginal bone level around implants—in particular that of the buccal bone—and for assessing the outcome of bone regenerative procedures [49, 55, 58, 64–72]. For instance, the outcome of lateral bone augmentation with autogenous and allogenic bone blocks was compared based on CBCT recorded post-operatively and after 6 months [72]. Specifically, bucco-oral cross-sections were generated at the center of the fixation screw, ensuring spatial reproducibility of the sections from the two observation periods; one mask overlapping the bone block and one the pristine bone were generated on the post-operative CBCT, where the boundaries of the block were clearly recognizable. Then the sum of these two regions was subtracted from the region of a single mask overlapping the bone tissues in the 6-month CBCT, where the interface of the bone block and the pristine bone was not recognizable anymore. Based on the assumption that the volume of the pristine bone is not really changing during the observation period, bone block resorption could be estimated (Fig. 10.14).

Although CBCT has indeed been proven to be very accurate in terms of distance measurements of anatomical landmarks and dimensions of bone defects [49, 55, 58, 65, 68], there are concerns regarding the diagnostic accuracy of CBCT to assess peri-implant bone defects and the marginal peri-implant bone level. In a methodological study, a good correlation between the measurements of bone levels in CBCT scans and histological sections was shown, but the radio-graphic peri-implant bone level estimated with CBCT was on average 1.12 mm higher than the true histological bone level [73]. Similar results have been shown in other studies with mean differences up to 2.6 mm between CBCT estimates and true bone levels [74–76]. The discrepancies between CBCT and true measurements can be explained by the variations in image sectioning and display settings, such as section thickness and mapping of scalar values stored within the displayed image (e.g., windowing/contrast control), which are shown to have a large impact on the characteristics of the final image [77], but also by the questionable image quality of CBCT in close proximity to dental implants, due to beam-hardening artifacts from the metal of the implants and/or reconstruction [78]. The beam-hardening artifacts within the reconstructed images are cupping and streak artifacts. Cupping artifacts occur when the multi-energetic radiation beam passes through a round or oval object with a high atomic number, e.g., metal. The softer part of the radiation beam is absorbed in the object, and the part of the beam that has succeeded in penetrating the center of the object will be harder when it reaches the receptor than the part passing through the edges. Streak artifacts appear as dark bands between two dense objects, such as two dental implants in the same jaw (Fig. 10.15).

Several factors seem to influence the diagnostic accuracy of CBCT with regard to buccal bone measurements at implant sites [79–86]. For example, in an ex vivo study with implants inserted flush to the alveolar crest of human man-
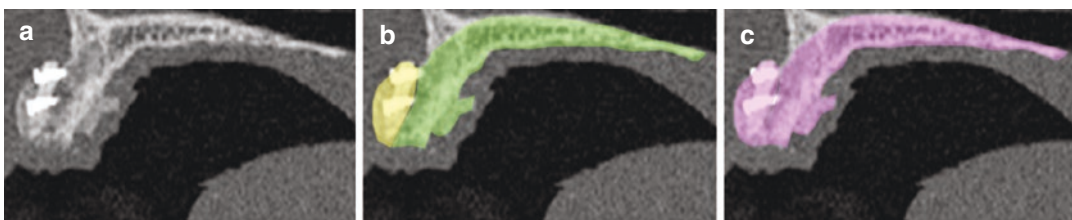

Fig. 10.14 Using the center of the fixation screw as a reference, spatial reproducibility of the sections between different observation periods is ensured; on the post-operative CBCT (**a**), where the boundaries of the block are clearly recognizable, masks overlapping the bone block and the pristine bone can be generated (**b**). The sum of the 2 regions is then subtracted from the region of a single mask overlapping the bone tissues in a later CBCT (**c**), where the interface of the bone block and the pristine bone is not recognizable anymore, to estimate bone block resorption
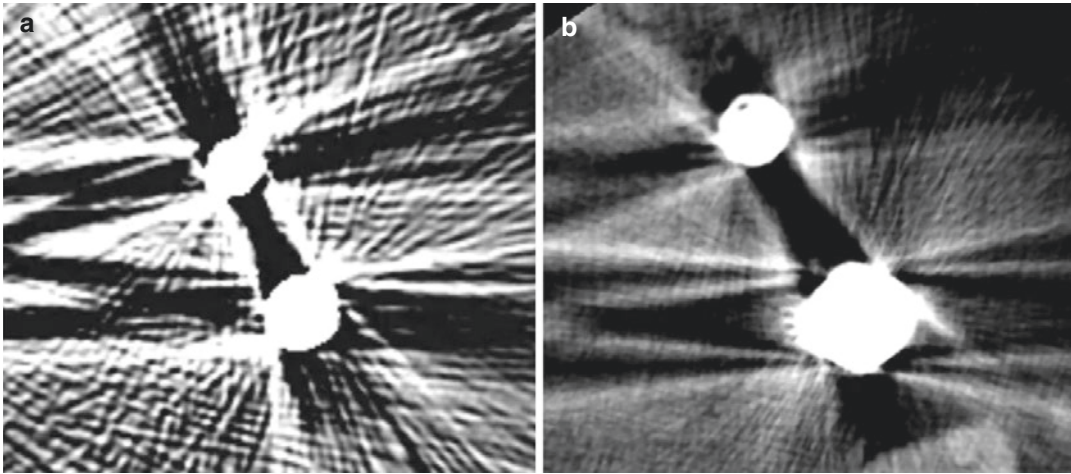
Fig. 10.15 Example of extreme beam-hardening artifacts between 2 dental implants in a CT (**a**) and CBCT (**b**) scan

dibles and harboring rectangular bone defects of varying dimensions at their buccal aspect, small volume defects (i.e., <3 × 3 mm) were much more frequently missed, compared with larger defects [82]. In two recently published in vitro evaluations in dry pig mandibles, it was demonstrated that various modifiable (e.g., the resolution and the image reconstruction thickness, the CBCT unit) and non-modifiable (e.g., the implant-abutment material, the number of implants in the field of view, the thickness of the buccal bone wall) factors influence the diagnostic accuracy of CBCT when assessing the buccal bone at implant sites [83, 84]. For instance, a high number of implants in the field-of-view, a low image resolution and reconstruction thickness, and the presence of a zirconium implant impair the correct diagnosis and/or measurements [83]. Further, a buccal bone wall less than 1 mm thick at implant sites was shown to significantly interfere with the ability of expert evaluators to discern whether or not a bone was present [83]. In another recently published ex vivo study [87], 9 out of 10 times a dehiscence was diagnosed although it did not exist when the buccal bone thickness was less than 1 mm, while when the buccal bone thickness was 1 mm or more, the presence of a dehiscence was wrongly attributed only in 20–30% of the cases (Fig. 10.16). In this context, previous reports indicate that the majority of extraction sites in the anterior regions of the mouth present a thin buccal wall; thus, such sites experience larger dimensional changes, i.e., volume loss in terms of "buccal collapse," compared with posterior sites where the buccal bone is often thicker (> 1 mm) [88, 89]. It may be expected therefore that also anterior implants often present with a buccal wall less than 1 mm thick at the crestal aspect. It appears therefore, reasonable to suggest that CBCT should not be used to assess the buccal bone level at implants inserted in narrow alveolar ridges, especially in the anterior regions of the mouth (Fig. 10.17).

CBCT has also been suggested as a method to assess bone quality, i.e., more or less dense trabecular bone, as an analog to conventional CT. Although the judgment of bone quality based on Hounsfield Unit values is well accepted for conventional CT imaging [90, 91], a similar correlation between gray values in CBCT scans and bone quality cannot be assumed. Several studies have tested the possibility to correlate quantitatively gray values of CBCT scans to bone quality [90, 92–94]. However, gray values of CBCT scans are strongly affected by the CBCT device, positioning of the patient, artifacts, and imaging parameters, which do not allow any meaningful use of CBCT for assessing bone quality.
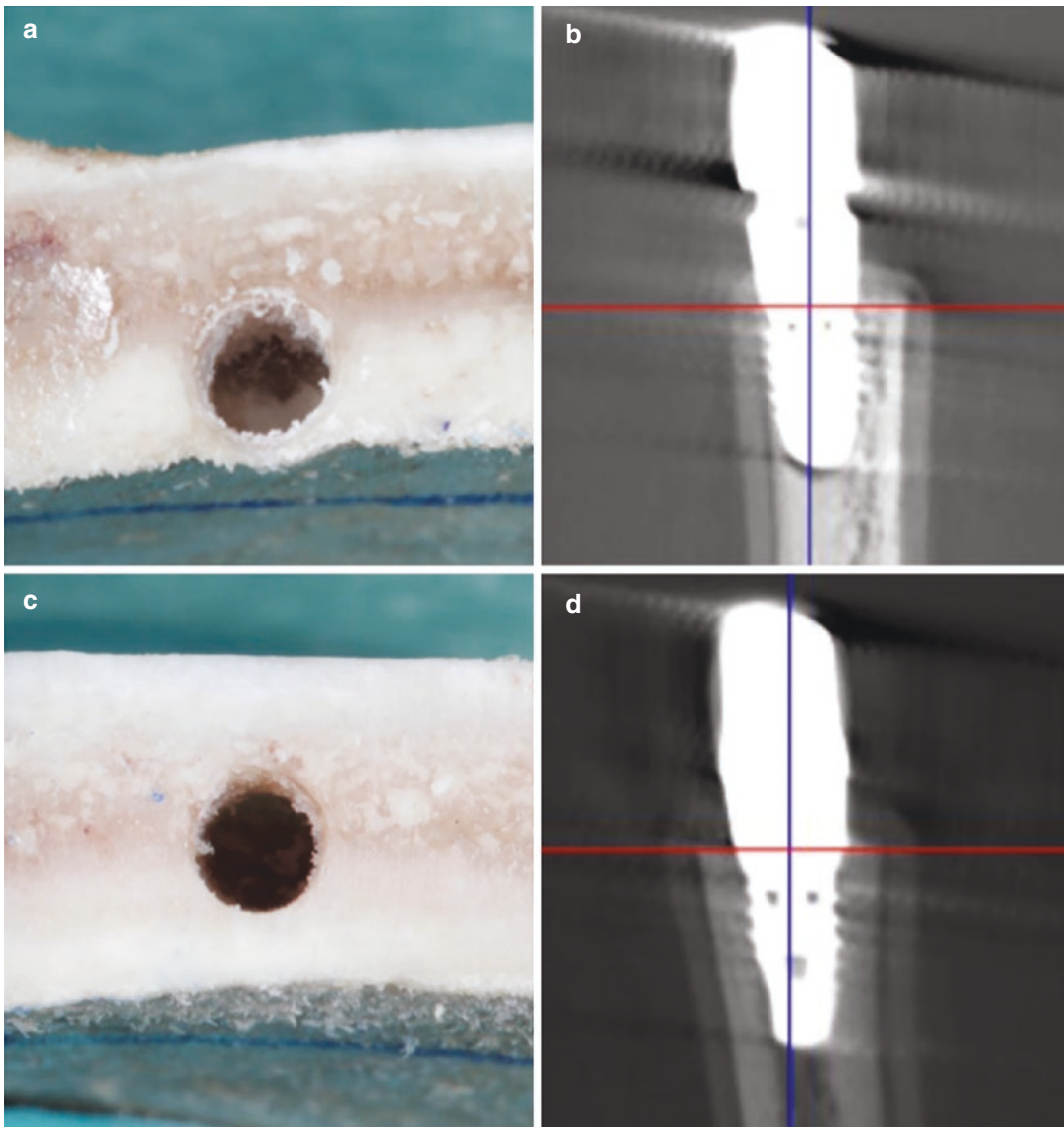
Fig. 10.16 A buccal bone thickness less than 1 mm (**a**) significantly interferes with the ability to discern whether the bone is present or absent in a CBCT scan (**b**), while a buccal bone >1 mm thick (**c**) is easier to identify (**d**). Note that the extra layer visible in the CBCT scans on the outside of the bone is a layer of pink wax imitating the soft tissue during the scan

In perspective, the use of CBCT is not recommended as a routine imaging technique for implant cases according to the European Guideline: Radiation Protection No. 172 [95]. Nevertheless, a recent study from Finland indicated a possible association between the reduced frequency of compensable malpractice claims related to dental implants and the increasing availability of CBCT technology [96].
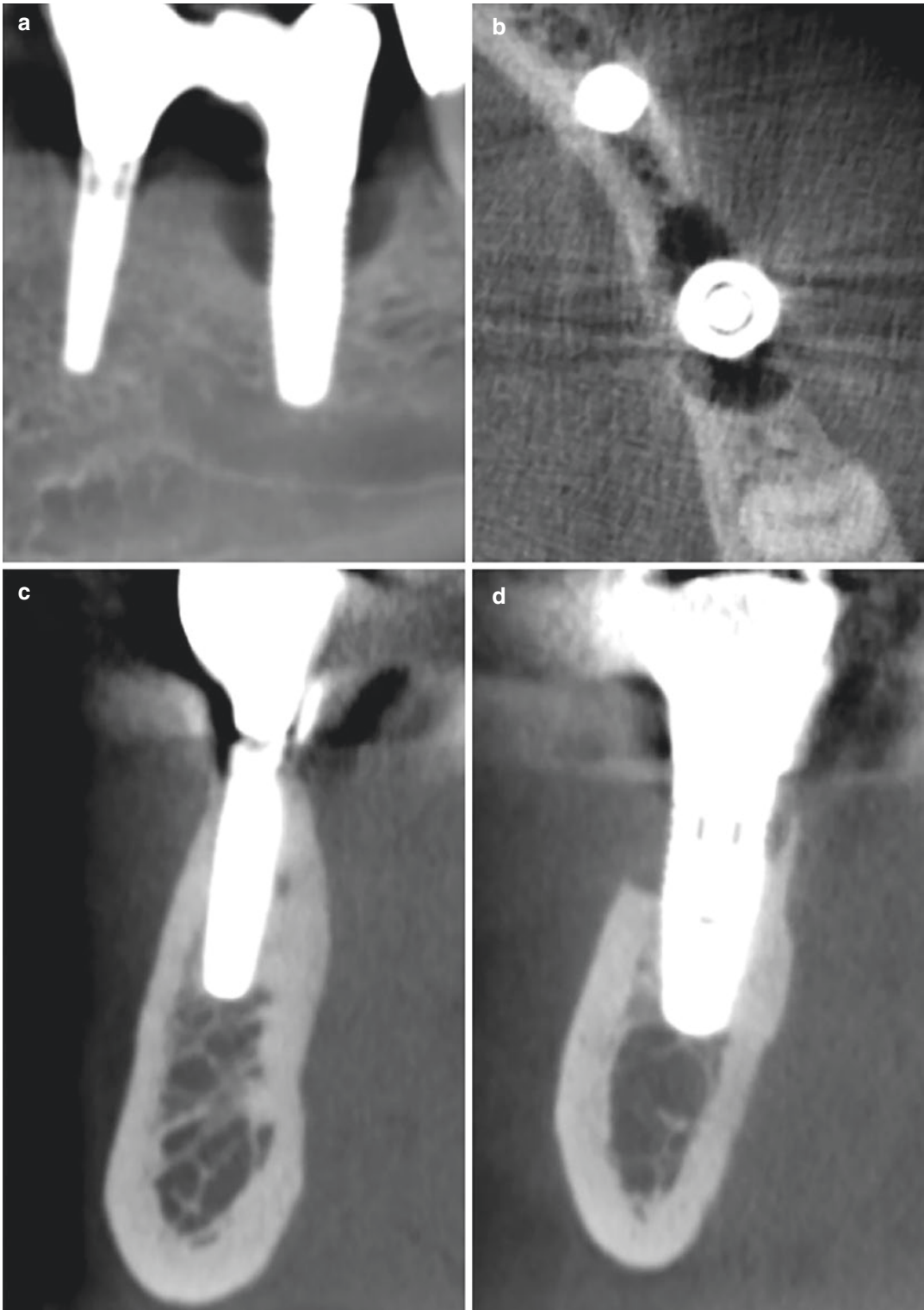
Fig. 10.17 Panoramic view (**a**), axial view (**b**), and cross-sectional view of the mesial (**c**; left implant in **a**) and distal (**d**; right implant in **a**) implant. Note that the level of the buccal bone at the mesial implant, where the bone is thin, cannot be clearly discerned, compared with that in the distal implant where the buccal bone is thick

10.4.2 MRI

Magnetic resonance imaging (MRI) provides an imaging modality free of ionizing radiation in contrast to conventional radiography or computed tomography (CT or CBCT), and it has been used for a long time in dentistry for imaging of temporomandibular joint (TMJ) disorders [97] REF SHOULD BE 96. The basic principle of MRI relies on the possibility of magnetizing atomic nuclei (protons), i.e., hydrogen atoms, which are found in different amounts in the human body. Hydrogen atoms are randomly orientated; however, they align parallel in the longitudinal axis of the body if an external magnetic field is turned on (resting alignment). This alignment can be disturbed by external radiofrequency (RF) waves. If the RF impulse is turned off, the protons return to their resting alignment by emission of RF energy, which is then captured by specific sensors and finally displayed as a grayscale image. Different relaxation times result in T1-weighted (longitudinal relaxation time) and T2-weighted (transverse relaxation time) images. They can be distinguished by, e.g., the cerebrospinal fluid, which appears dark (T1) or light (T2) [98].

Advances in MRI technology and the development of ultra-short or zero echo time sequences have broadened its spectrum for imaging, including hard tissues, e.g., bones, which have short T2 relaxation rates [99, 100], and thus the use of MRI is currently explored also within implant dentistry. MRI allows the visualization of cortical and trabecular bone of the maxilla/mandible, maxillary sinus, teeth, pulp chamber, periodontal space, and critical structures, including the lingual nerve and inferior alveolar nerve (IAN), mental foramen, and the incisive nerve (Fig. 10.18) [99, 101–104].

A clear depiction of bone and teeth is crucial if MRI should be considered a reasonable diagnostic method for the planning, placing, and monitoring of implants in dentistry. The appearance of bone in MRI is entirely different from CT and CBCT imaging, e.g., cortical bone consists by its nature of a relatively low number of nuclei (protons in water) that can be magnetized. As a result, cortical bone is displayed as a dark region corresponding to a signal void (Fig. 10.19) [105].

Recent studies considered MRI as an option for preoperative implant planning and even the fabrication of surgical guides. A comparison of virtually planned implants in MRI and CBCT datasets demonstrated no significant differences relating to the apical and coronal position of the implant. However, when comparing the distance from the alveolar crest to the mandibular canal (visualized in CBCT) with that to the inferior alveolar nerve (visualized in MRI), it was found
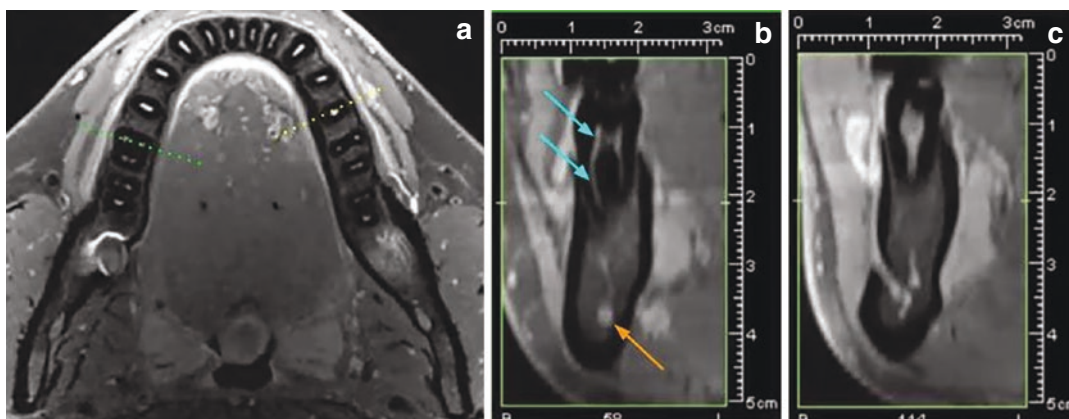

Fig. 10.18 Axial view of the mandible (**a**). Note the hypointense signal of the cortical bone and teeth in contrast to the hyperintense signal of the pulp. (**b**) The pulp and the root canals of the mesial root (first molar) are clearly depicted (turquoise arrows). The inferior alveolar nerve/neurovascular bundle can be directly visualized (orange arrow). (**c**) Visualization of the mental foramen in MRI
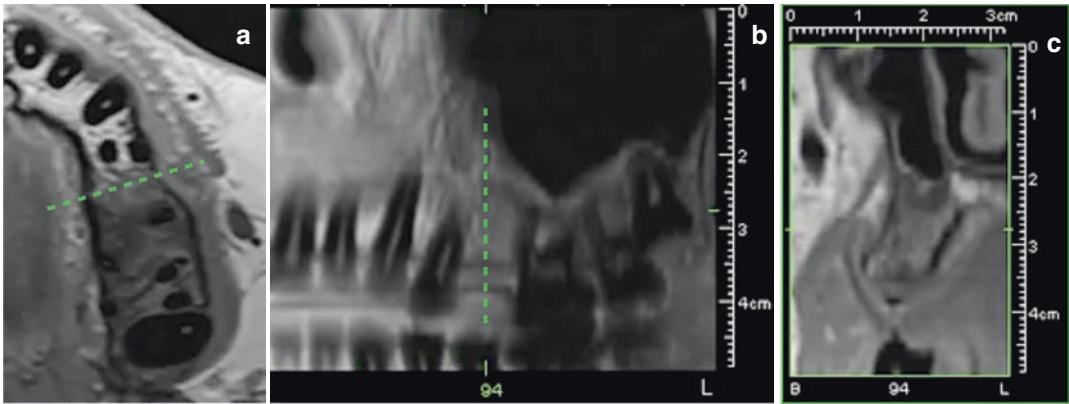
Fig. 10.19 Preoperative axial view of the implant planning site (**a**), the green dotted line on the panoramic-view (**b**) indicates the slice of orthoradial reconstruction (**c**) which allows measuring of the bone quantity

that it was significantly larger (by 1.3 ± 0.81 mm) in the MRI, i.e., implant planning by means of MRI would accept the installation of longer implants [106]. Nevertheless, there is no verification of the true distance from the alveolar crest to the inferior alveolar nerve, in vivo or in vitro.

MRI-based implant planning can be verified when this information is transferred to surgical guides and ultimately used for implant placement. Fully guided implant placement based on information from MRI has been successfully performed in vivo in five patients [107] and in vitro involving 16 human cadaver hemi-mandibles [108]. Planning and printing of the surgical guides were based solely on MRI data and optical surface scans. The in-vitro study design allowed comparison of the planned (MRI) and the final implant position (hemi-mandible) by postoperative CBCT and optical scans: deviations were 1.34 ± 0.84 and 1.03 ± 0.46 mm at the implant shoulder and 1.41 ± 0.88 and 1.28 ± 0.52 mm at the implant apex, respectively. Angular deviations of the implant axis were $4.84 \pm 3.18°$ and $4.21 \pm 2.01°$, respectively [108]. Despite the feasibility of using MRI for preoperative planning, it is evident that MRI (still) requires an additional optical scan for virtual implant planning. Teeth surfaces are depicted with insufficient accuracy, and alignment is basically based on soft tissue (e.g., keratinized mucosal surface) and/or radio-opaque markers [108]. A lower accuracy for MRI compared to CBCT for tooth surface reconstruc-

tion has been demonstrated: geometric deviations were 0.26 ± 0.08 and 0.1 ± 0.04 RMS, [1] respectively [109].

In this context, artifacts may occur in MRI similarly to CT and CBCT and can strongly impair the diagnostic value of the image. They can be classified according to their origin as patient (e.g., motion, metal artifact), signal-processing (e.g., chemical shift artifact, partial volume artifact), or hardware-related (e.g., external magnetic field inhomogeneity, gradient field artifacts) [110]. Metal artifacts result from the different magnetic susceptibility of adjacent tissues, e.g., the interface between a dental implant and bone, which can lead to (total) signal loss. Furthermore, the prosthetic restoration material also induces susceptibility artifacts. Resin as a crown material hardly produced any artifacts, while precious metal-ceramic, ceramic, and zirconia demonstrated minor artifacts. Furthermore, the number of crowns significantly affects the extension of the artifacts measured by area [111]. Similar results have been reported for implants restored with various types of crowns: monolithic zirconia crowns attached to zirconia implants demonstrated the least artifacts, followed by porcelain-fused-to-zirconia and monolithic zirconia crowns on titanium implants. Most artifacts were reported for titanium implants in combination with non-precious alloys [112]. Therefore,

---

[1]*RMS* root mean square.

patients considered for dental MRI should be screened for metal-containing fillings/restorations, orthodontic wires, or dental implants that may interfere with the region of interest.

The obvious advantage of having no ionizing radiation makes MRI a reasonable alternative for monitoring dental implants and 3D defect imaging in case of peri-implant diseases. However, the use of MRI appears more relevant for zirconia implants (Fig. 10.20), which are depicted more clearly, compared to titanium or titanium-zirconia implants, both demonstrating signal voids due to susceptibility artifacts [113] (Fig. 10.21). The distribution of artifacts is smaller for zirconia than titanium implants, irrespective of the implant's geometry or the site of measurement
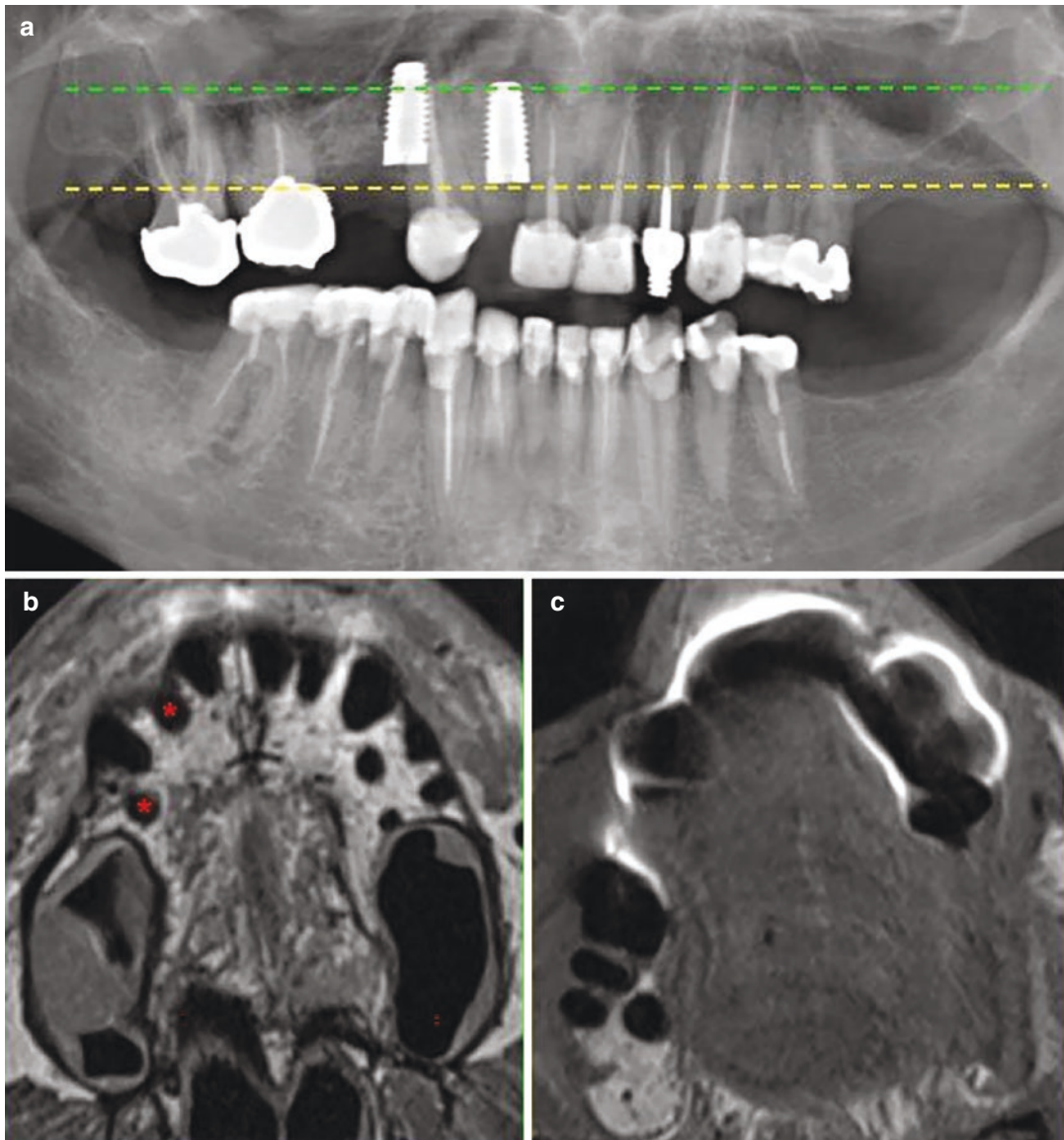

Fig. 10.20 Postoperative panoramic X-ray (**a**) and MRI (**b**, **c**) following placement of two zirconia implants. Note, MRI verifies that zirconia implants (red asterisks) do not interfere with adjacent teeth, despite the presence (**c**) of susceptibility artifacts
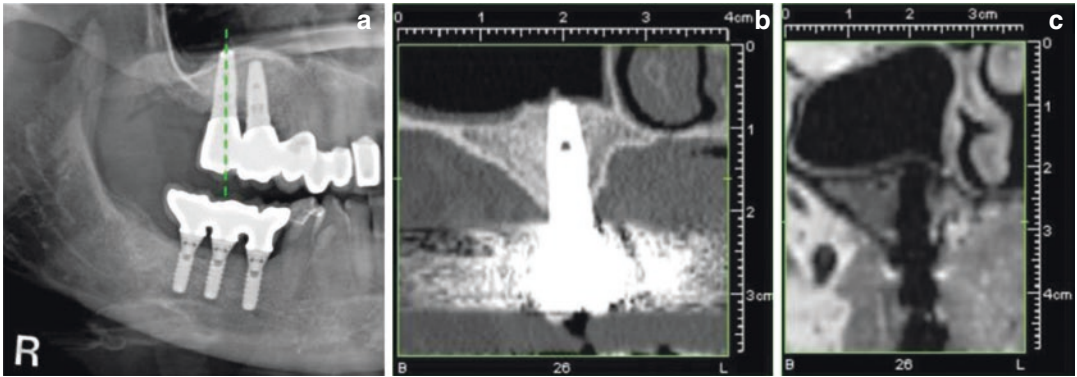
Fig. 10.21 Panoramic X-ray indicating titanium implants with zirconia crowns (**a**); the green dotted line demonstrates the orthoradial view in CT (**b**) and MRI (**c**) of implant #16. Note the strong and minor artifacts induced by the zirconia crown in CT (**b**) and MRI (**c**), respectively. In addition, the titanium implant appears slightly distorted in MRI (**c**) in comparison to CT (**b**) imaging

(e.g., buccal vs. lingual) [114]. Distance measurements of zirconia implants indicated a high correlation between MRI and CBCT, which is also reflected by the longitudinal and transversal accuracy of the actual implant's size, i.e., 0.8% and 2.3%, respectively. In contrast, the size of titanium implants was overestimated by 29.7% and 36.9%, respectively [115]. Both zirconia and titanium implants appear as hypointense structures, i.e., signal voids; however, artifacts were more significant on T2- than T1-weighted images [116]. However, similar results for MRI and CBCT have been demonstrated for the judgment of large peri-implant defects (i.e., 3 mm) around zirconia implants in-vitro, both outperforming intraoral radiographs. Nevertheless, intraoral radiographs performed better in detecting small defect sizes (i.e., 1 mm) [117].

Besides inherent artifacts, MRI remains a valuable diagnostic tool if an injury of the infe-

rior alveolar nerve following implant placement is clinically suspected. MRI allows direct visualization of the inferior alveolar nerve in contrast to CT/CBCT, which may miss the protrusion of an implant into the mandibular canal if its corticalization is insufficient [103, 118]. MRI has also been investigated for the evaluation of bone augmentations, particularly maxillary sinus floor augmentations (MSFA) and onlay grafts. Vertical bone height changes following MSFA can be assessed safely using MRI (Fig. 10.22) [119]. Furthermore, the healing of autologous onlay bone grafts in their early stages was visualized by MRI in combination with an intraoral coil. Cortical and cancellous bone could be differentiated, and the volume of the block graft was calculated. Osteosynthesis screws were displayed as signal voids encircled by a thin fringe [120].
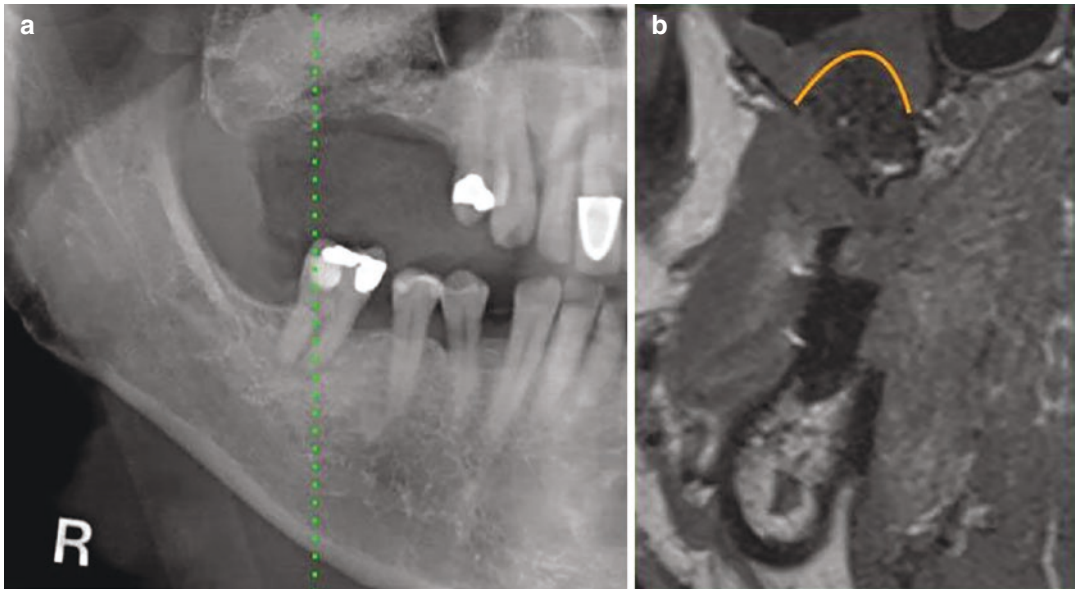
Fig. 10.22 Panoramic X-ray following MSFA (**a**) and MRI 1 day postoperatively to verify possible dislocation of the graft into the maxillary sinus (**b**). Note: the green dotted line (**a**) indicates the coronal view (**b**) of the MRI, the orange line indicates the upper border of the graft

10.5   Subtraction Radiography

Subtraction radiography was introduced in the 1930s and is a well-established method for the detection of bone changes in serial radiographs. During the 1990s subtraction radiography has also been used in dental research, including assessment of morphologic changes and bone formation and remodeling of extraction sites [121] as well as for the follow-up evaluation of implants [122–126].

Manual, semi-, or fully-automated systems for subtraction radiography exist. Briefly, subtraction radiography is based on the principle that a computer program simply calculates the pixel-pixel difference between two digital radiographs. Some systems are more advanced and, based on contrast adaption, subtract the gray shade value of each pixel in one image from the corresponding pixel value in another image, resulting in the subtraction image that represents the differences in gray shades between the pixels values in two radiographs. Provided that the two radiographs to be subtracted are recorded with standardized projection geometry and properly aligned, the differ-

ences in gray shades in the bone may be interpreted as differences in bone mineral content. For example, Reddy et al. [126] demonstrated high repeatability of a semi-automated computer-assisted method used for measuring bone loss around implants. In another study, Brägger et al. [122] demonstrated peri-implant density changes during the early healing phase and ligature-induced peri-implantitis in an animal model, as well as cases documenting the loss of peri-implant bone density associated with infection or increase in density caused by remodeling after functional loading of an implant with a single crown.

Despite the fact that subtraction radiography has been advocated for the detection of minor bone changes, one must be aware of the shortcomings of this technique. The major limitation of subtraction radiography when analyzing changes in a given bone defect is that the visualization depends on the bucco-oral width of this defect. Total bone fill with uniform density in a bowl- or cone-shaped defect, as in an augmented peri-implantitis defect or an immediate implant placed in an extraction socket, respectively, may

be visualized only in the coronal part. This is because the width of the defect at that point makes up a larger fraction of the total width of the alveolar bone at its coronal aspect as compared with the apical aspect. Likewise, one must bear in mind that the subtraction image is a product of remodeling of the bone walls on the buccal and lingual/palatal aspect of the defect on one hand and bone formation/resorption within the defect on the other; obviously, it may not be possible to distinguish among these biological phenomena.

In perspective, due to the above shortcomings, together with the high costs associated with dedicated software and the cumbersome training needed, as well as the time-consuming use of the technique and the fact that the new digital systems give better possibilities for direct visualization of shades of gray, subtraction radiography has not achieved widespread use in implant research.

10.6   Micro CT

Histomorphometry, i.e., the quantitative assessment of histological sections from non-decalcified samples containing the implant and surrounding tissues, is commonly used to assess the amount/extent of osseointegration, i.e., the direct BIC; this method allows also the assessment of the bone type and mineralization level and is considered the gold standard [127–129]. However, histomorphometry—and histology in general—is a destructive technique, and once the sections are cut, it is not possible anymore to analyze the sample in any other direction than that of the section plane. Further, non-decalcified sections have the additional drawback that a rather significant volume of the specimen/implant is lost during the cutting process, due to the physical thickness of the cutting knife itself and the subsequent grinding/polishing of the section. Thus, from standard-size implants, only 1–2 sections are usually available for histomorphometric evaluation, which does not allow an accurate 3-D assessment of bone architecture.

In this context, microcomputed tomography (µCT) is a high-resolution 3-D imaging technique and is an established tool to assess bone ex vivo, as an alternative method to bone histomorphometry [130–136]. µCT offers the main advantages—compared to histomorphometry—of non-destructive assessment of bone morphology, and that relatively large volumes of interest can be analyzed in a truly 3-D way. In addition, the whole process of analysis can start immediately after the tissue samples are available and thus a faster analysis can be achieved. µCT has also been suggested to assess BIC [137–140]. A few studies have shown a good correlation between BIC estimates from µCT and from histomorphometry with relatively small discrepancies—either showing under- or overestimation of BIC with µCT [139, 141]. Other studies, however, have observed large differences between BIC values from µCT and histomorphometry, which are attributed to the presence of similar type—but of less magnitude—of artifacts, as those described above for CBCT (i.e., beam-hardening artifacts) [142, 143] (Fig. 10.23).

Conventional µCT devices are limited by the maximum current of the X-ray tube; this in turn is limited by physical constraints and the integration time that is directly related to the total scanning time. A way to improve resolution, voxel information content, and to limit drastically the beam-hardening effect is to use synchrotron radiation (SR) as the X-ray source. The beam generated from an SR source is very brilliant, characterized by a high flux of photons; it is, therefore, possible to filter the beam using a monochromator so that only a specific, narrow range of energies is utilized. As the intensity of the original beam is very high, the remaining monochromatic flux has enough photons, all characterized by the same energy level, to generate an excellent signal-to-noise ratio (SNR) with virtually the absence of beam hardening. Further, in contrast with conventional µCT, where the beam has either a fan shape or a cone shape, the incident beam of SR is long, the source divergence is small, and, the X-rays are nearly parallel. These characteristics of SRµCT scanning
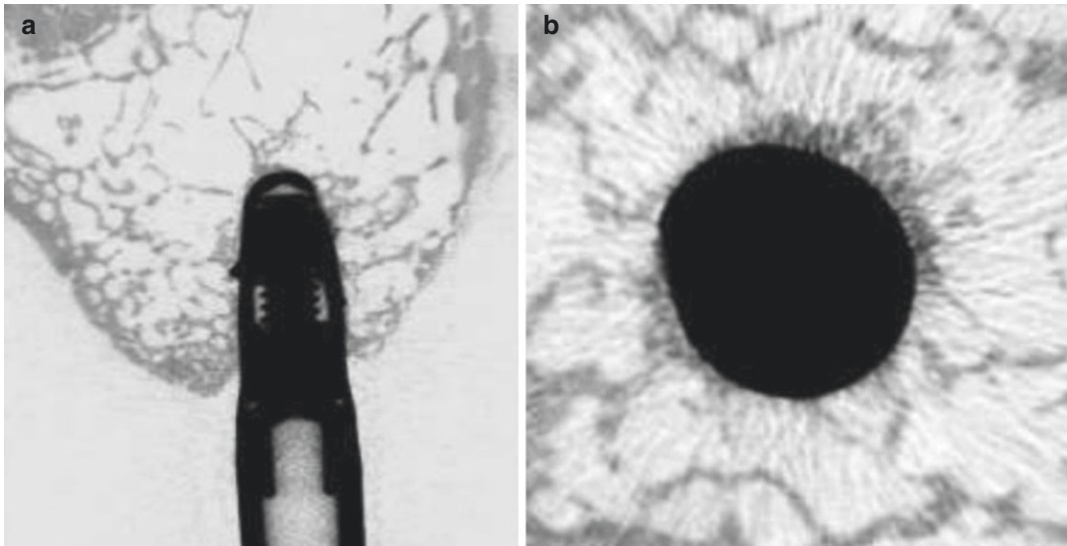
Fig. 10.23 Bucco-palatal (**a**) and axial (**b**) section from the maxilla of a macaca fascicularis monkey, containing a titanium dental implant scanned with conventional μCT. Precise BIC estimation appears compromised due to the presence of beam-hardening artifacts
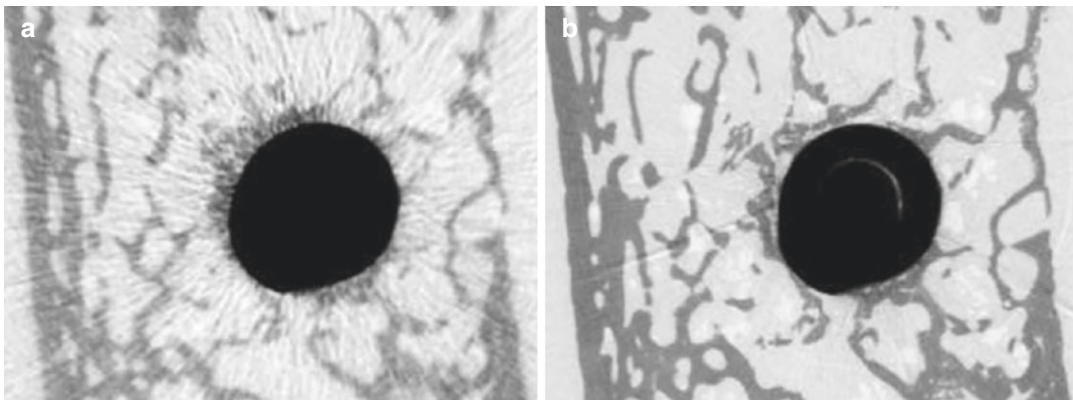

Fig. 10.24 Cross-sections from the maxilla of a macaca fascicularis monkey containing a titanium dental implant scanned with conventional μCT (**a**) and SRμCT. Note the extent of beam-hardening artifacts in the μCT image (**a**), that are almost absent in the image from the SR-based scanner (**b**)

allow for higher resolution, which can be up to 1/10 of the 1 μm range [144]. Consequently, the images obtained from SRμCT scanning are less noisy and the bony edges are sharper than the ones generated by the conventional μCT (Fig. 10.24).

Thus, with limited beam-hardening artifacts in SRμCT scans, better visualization of the relationship of the bone tissue to the implant is possible (Fig. 10.25). Nevertheless, and although it may

seem reasonable that a better estimation of BIC would also be possible with SRμCT compared with conventional μCT, a recent study showed a discrepancy of 5–15% between SRμCT and histology in terms of BIC [145]. In perspective, μCT and SRμCT facilitate improved visualization and understanding of tissues and implants in 3-D (Fig. 10.26) but are still not considered as precise as classic histomorphometry using light microscopy to assess osseointegration [146].
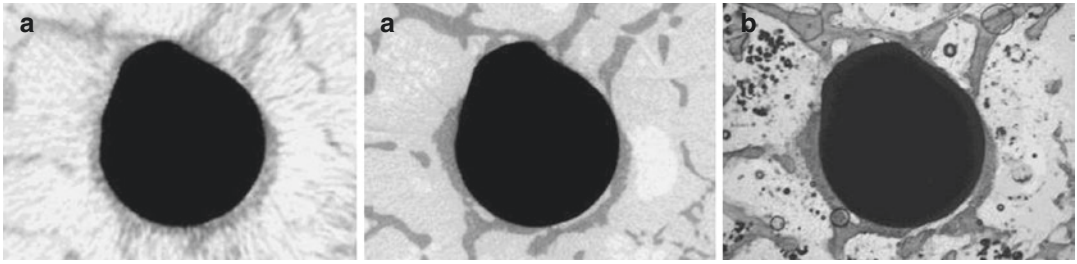
Fig. 10.25 Assessment of BIC is clearly compromised due to beam-hardening artifacts in a section from a conventional μCT (**a**), while BIC in a section from a SRμCT (**b**) seems to correspond well to that estimated in a non-decalcified histological section (**c**)
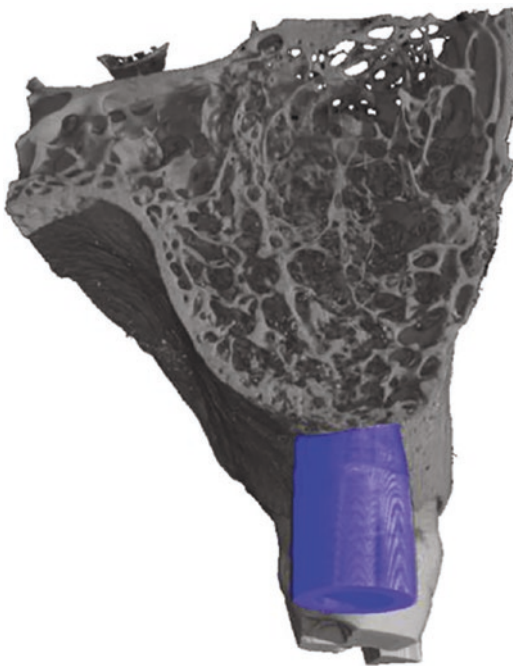

Fig. 10.26 3-D reconstruction of an aspect of the maxilla of a macaca fascicularis monkey containing a titanium dental implant scanned with SRμCT, where even some of the smallest trabeculae are clearly visible

10.7 Conclusion

Intraoral periapical radiographs provide the best spatial resolution and are recommended for implant planning in simple implant cases where clinical measures suffice to estimate bone thickness and no challenges exist with respect to interference with anatomic structures, e.g., the mandibular canal. Periapical radiography is most often the method of choice for clinical monitoring and research purposes when assessing the peri-implant bone level. A pre-requisite for assessing the peri-implant bone level with relatively good precision in periapical radiographs is that images are calibrated and that sharp threads on both sides of the implant are displayed. This can readily be achieved with the RB-RB/LB-LB mnemonic rule. Panoramic images are often appropriate for treatment planning, i.e., for selecting the implant size and position, in most of the cases where more than one implant is planned or in cases with a risk for interference with anatomic structures; the distortion and magnification of the panoramic image should be taken into consideration by a calibration procedure. However, when a clinical examination or the panoramic radiograph may indicate inadequate bone volume for implant installation or anatomical aberrations, which may require special attention or modification of the surgical technique, a CBCT should be obtained. However, panoramic images and CBCT are not appropriate for routine monitoring or for research purposes for assessing the peri-implant bone level, because the bone-to-implant interface is not clearly visualized. Similarly, although μCT and SRμCT are precise for bone volume estimations, the technology cannot yet be used to assess BIC as precisely as with histomorphometry.

References

1. Coli P, Christiaens V, Sennerby L, Bruyn H. reliability of periodontal diagnostic tools for monitoring peri-implant health and disease. Periodontol 2000. 2017;73:203–17. https://doi.org/10.1111/prd.12162.

2. Koldsland OC, Scheie AA, Aass AM. Prevalence of peri-implantitis related to severity of the disease with different degrees of bone loss. J Periodontol. 2010;81:231–8. https://doi.org/10.1902/jop.2009.090269.

3. Fuglsig JMCES, Thorn JJ, Ingerslev J, Wenzel A, Spin-Neto R. Long term follow-up of titanium implants installed in block-grafted areas: a systematic review. Clin Implant Dent Relat Res. 2018;20:1036–46. https://doi.org/10.1111/cid.12678.

4. Pepelassi EA, Diamanti-Kipioti A. Selection of the most accurate method of conventional radiography for the assessment of periodontal osseous destruction. J Clin Periodontol. 1997;24:557–67.

5. Larheim TA, Eggen S. Determination of tooth length with a standardized paralleling technique and calibrated radiographic measuring film. Oral Surg Oral Med Oral Pathol. 1979;48:374–8.

6. Sonick M, Abrahams J, Faiella RA. A comparison of the accuracy of periapical, panoramic, and computerized tomographic radiographs in locating the mandibular canal. Int J Oral Maxillofac Implants. 1994;9:6.

7. Schropp L, Stavropoulos A, Gotfredsen E, Wenzel A. Calibration of radiographs by a reference metal ball affects preoperative selection of implant size. Clin Oral Investig. 2009;13:375–81. https://doi.org/10.1007/s00784-009-0257-5.

8. Berglundh T, Armitage G, Araujo MG, et al. Peri-implant diseases and conditions: consensus report of workgroup 4 of the 2017 world workshop on the classification of periodontal and Peri-implant diseases and conditions. J Clin Periodontol. 2018;45(Suppl 20):S286–91. https://doi.org/10.1111/jcpe.12957.

9. Borrow JW, Smith JP. Stent marker materials for computerized tomograph-assisted implant planning. Int J Periodontics Restorative Dent. 1996;16:60–7.

10. Gröndahl K, Ekestubbe A, Gröndahl H. Postoperative radiographic examinations. In: Gröndahl K, Ekestubbe A, Gröndahl H, editors. Radiography in oral endosseous prosthetics; 1996. p. 111–26.

11. Schropp L, Stavropoulos A, Spin-Neto R, Wenzel A. Evaluation of the RB-RB/LB-LB mnemonic rule for recording optimally projected intraoral images of dental implants: an in vitro study. Dentomaxillofac Radiol. 2012;41:298–304. https://doi.org/10.1259/dmfr/20861598.

12. Sewerin I. Device for serial intraoral radiography with controlled projection angles. Tandlaegebladet. 1990;94:613–7.

13. Schropp L, Stavropoulos A, Spin-Neto R, Wenzel A. Implant image quality in dental radiographs recorded using a customized imaging guide or a standard film holder. Clin Oral Implants Res. 2012;23:55–9. https://doi.org/10.1111/j.1600-0501.2011.02180.x.

14. Abrahamsson I, Berglundh T, Moon IS, Lindhe J. Peri-implant tissues at submerged and non-submerged titanium implants. J Clin Periodontol. 1999;26:600–7.

15. Gotfredsen K, Berglundh T, Lindhe J. Bone reactions at implants subjected to experimental peri-implantitis and static load. A study in the dog. J Clin Periodontol. 2002;29:144–51.

16. Duyck J, Corpas L, Vermeiren S, et al. Histological, histomorphometrical, and radiological evaluation of an experimental implant design with a high insertion torque. Clin Oral Implants Res. 2010;21:877–84. https://doi.org/10.1111/j.1600-0501.2010.01895.x.

17. Albouy JP, Abrahamsson I, Persson LG, Berglundh T. Spontaneous progression of peri-implantitis at different types of implants. An experimental study in dogs. I: clinical and radiographic observations. Clin Oral Implants Res. 2008;19:997–1002. https://doi.org/10.1111/j.1600-0501.2008.01589.x.

18. Albouy JP, Abrahamsson I, Persson LG, Berglundh T. Spontaneous progression of ligatured induced peri-implantitis at implants with different surface characteristics. An experimental study in dogs II: histological observations. Clin Oral Implants Res. 2009;20:366–71.

19. Lang NP, Wetzel AC, Stich H, Caffesse RG. Histologic probe penetration in healthy and inflamed peri-implant tissues. Clin Oral Implants Res. 1994;5:191–201.

20. Schou S, Holmstrup P, Stoltze K, Hjørting-Hansen E, Fiehn NE, Skovgaard LT. Probing around implants and teeth with healthy or inflamed peri-implant mucosa/gingiva. A histologic comparison in cynomolgus monkeys (Macaca fascicularis). Clin Oral Implants Res. 2002;13:113–26.

21. Serino G, Turri A, Lang NP. Probing at implants with peri-implantitis and its relation to clinical peri-implant bone loss. Clin Oral Implants Res. 2013;24:91–5. https://doi.org/10.1111/j.1600-0501.2012.02470.x.

22. Borg E, Gröndahl K, Persson LG, Gröndahl HG. Marginal bone level around implants assessed in digital and film radiographs: in vivo study in the dog. Clin Implant Dent Relat Res. 2000;2:10–7.

23. De Smet E, Jacobs R, Gijbels F, Naert I. The accuracy and reliability of radiographic methods for the assessment of marginal bone level around oral implants. Dentomaxillofac Radiol. 2002;31:176–81. https://doi.org/10.1038/sj/dmfr/4600694.

24. Kavadella A, Karayiannis A, Nicopoulou-Karayianni K. Detectability of experimental peri-implant cancellous bone lesions using conventional and direct digital radiography. Aust Dent J. 2006;51:180–6.

25. Matsuda Y, Hanazawa T, Seki K, Sano T, Ozeki M, Okano T. Accuracy of Digora system in detecting artificial peri-implant bone defects. Implant Dent. 2001;10:265–71.

26. Mörner-Svalling AC, Tronje G, Andersson LG, Welander U. Comparison of the diagnostic potential of direct digital and conventional intraoral radiography in the evaluation of peri-implant conditions. Clin Oral Implants Res. 2003;14:714–9.

27. Akesson L, Håkansson J, Rohlin M. Comparison of panoramic and intraoral radiography and pocket probing for the measurement of the marginal bone level. J Clin Periodontol. 1992;19:326–32.

28. Hämmerle CH, Ingold HP, Lang NP. Evaluation of clinical and radiographic scoring methods before and after initial periodontal therapy. J Clin Periodontol. 1990;17:255–63.

29. Ferreira CE, Novaes AB, Haraszthy VI, Bittencourt M, Martinelli CB, Luczyszyn SM. A clinical study of 406 sinus augmentations with 100% anorganic bovine bone. J Periodontol. 2009;80:1920–7. https://doi.org/10.1902/jop.2009.090263.

30. Lai HC, Zhuang LF, Lv XF, Zhang ZY, Zhang YX, Zhang ZY. Osteotome sinus floor elevation with or without grafting: a preliminary clinical trial. Clin Oral Implants Res. 2010;21:520–6. https://doi.org/10.1111/j.1600-0501.2009.01889.x.

31. Batenburg RH, Stellingsma K, Raghoebar GM, Vissink A. Bone height measurements on panoramic radiographs: the effect of shape and position of edentulous mandibles. Oral Surg Oral Med Oral Pathol Oral Radiol Endod. 1997;84:430–5.

32. Gomez-Roman G, Lukas D, Beniashvili R, Schulte W. Area-dependent enlargement ratios of panoramic tomography on orthograde patient positioning and its significance for implant dentistry. Int J Oral Maxillofac Implants. 1999;14:248–57.

33. Riecke B, Friedrich RE, Schulze D, et al. Impact of malpositioning on panoramic radiography in implant dentistry. Clin Oral Investig. 2015;19:781–90. https://doi.org/10.1007/s00784-014-1295-1.

34. Sadat-Khonsari R, Fenske C, Behfar L, Bauss O. Panoramic radiography: effects of head alignment on the vertical dimension of the mandibular ramus and condyle region. Eur J Orthod. 2012;34:164–9. https://doi.org/10.1093/ejo/cjq175.

35. Jacobs R, van Steenberghe D. Radiographic indications and contra-indication for implant placement. In: Jacobs R, van Steenberghe D, editors. Radiographic planning and assessment of endosseous oral implants; 1998. p. 45–58.

36. Angelopoulos C, Thomas SL, Thomas S, et al. Comparison between digital panoramic radiography and cone-beam computed tomography for the identification of the mandibular canal as part of presurgical dental implant assessment. J Oral Maxillofac Surg. 2008;66:2130–5. https://doi.org/10.1016/j.joms.2008.06.021.

37. Bolin A, Eliasson S, von Beetzen M, Jansson L. Radiographic evaluation of mandibular posterior implant sites: correlation between panoramic and tomographic determinations. Clin Oral Implants Res. 1996;7:354–9.

38. Bou Serhal C, Jacobs R, Flygare L, Quirynen M, van Steenberghe D. Perioperative validation of localisation of the mental foramen. Dentomaxillofac Radiol. 2002;31:39–43. https://doi.org/10.1038/sj/dmfr/4600662.

39. Lam EW, Ruprecht A, Yang J. Comparison of two-dimensional orthoradially reformatted computed tomography and panoramic radiography for dental implant treatment planning. J Prosthet Dent. 1995;74:42–6.

40. Lindh C, Petersson A. Radiologic examination for location of the mandibular canal: a comparison between panoramic radiography and conventional tomography. Int J Oral Maxillofac Implants. 1989;4:249–53.

41. Lindh C, Petersson A, Klinge B. Visualisation of the mandibular canal by different radiographic techniques. Clin Oral Implants Res. 1992;3:90–7.

42. Lindh C, Petersson A, Klinge B. Measurements of distances related to the mandibular canal in radiographs. Clin Oral Implants Res. 1995;6:96–103.

43. Madrigal C, Ortega R, Meniz C, López-Quiles J. Study of available bone for interforaminal implant treatment using cone-beam computed tomography. Med Oral Patol Oral Cir Bucal. 2008;13:E307–12.

44. Tal H, Moses O. A comparison of panoramic radiography with computed tomography in the planning of implant surgery. Dentomaxillofac Radiol. 1991;20:40–2. https://doi.org/10.1259/dmfr.20.1.1884852.

45. Fuhrmann R, Bücker A, Diedrich P. Radiological assessment of artificial bone defects in the floor of the maxillary sinus. Dentomaxillofac Radiol. 1997;26:112–6. https://doi.org/10.1038/sj.dmfr.4600223.

46. Fuhrmann RA, Wehrbein H, Langen HJ, Diedrich PR. Assessment of the dentate alveolar process with high resolution computed tomography. Dentomaxillofac Radiol. 1995;24:50–4. https://doi.org/10.1259/dmfr.24.1.8593909.

47. Fuhrmann RA, Bücker A, Diedrich PR. Furcation involvement: comparison of dental radiographs and HR-CT-slices in human specimens. J Periodontal Res. 1997;32:409–18.

48. Langen HJ, Fuhrmann R, Diedrich P, Günther RW. Diagnosis of infra-alveolar bony lesions in the dentate alveolar process with high-resolution computed tomography. Experimental results. Invest Radiol. 1995;30:421–6.

49. Stavropoulos A, Wenzel A. Accuracy of cone beam dental CT, intraoral digital and conventional film radiography for the detection of periapical lesions. An ex vivo study in pig jaws. Clin Oral Investig. 2007;11:101–6. https://doi.org/10.1007/s00784-006-0078-8.

50. Tammisalo T, Luostarinen T, Vähätalo K, Tammisalo EH. Comparison of periapical and detailed narrow-beam radiography for diagnosis of periapical bone

lesions. Dentomaxillofac Radiol. 1993;22:183–7. https://doi.org/10.1259/dmfr.22.4.8181644.

51. Velvart P, Hecker H, Tillinger G. Detection of the apical lesion and the mandibular canal in conventional radiography and computed tomography. Oral Surg Oral Med Oral Pathol Oral Radiol Endod. 2001;92:682–8. https://doi.org/10.1067/moe.2001.118904.

52. Liang X, Jacobs R, Hassan B, et al. A comparative evaluation of cone beam computed tomography (CBCT) and multi-slice CT (MSCT) part I. on subjective image quality. Eur J Radiol. 2010;75:265–9. https://doi.org/10.1016/j.ejrad.2009.03.042.

53. Nardi C, Talamonti C, Pallotta S, et al. Head and neck effective dose and quantitative assessment of image quality: a study to compare cone beam CT and multislice spiral CT. Dentomaxillofac Radiol. 2017;46:20170030. https://doi.org/10.1259/dmfr.20170030.

54. Harris D, Horner K, Gröndahl K, et al. E.a.O. guidelines for the use of diagnostic imaging in implant dentistry 2011. A consensus workshop organized by the European Association for Osseointegration at the Medical University of Warsaw. Clin Oral Implants Res. 2012;23:1243–53. https://doi.org/10.1111/j.1600-0501.2012.02441.x.

55. Correa LR, Spin-Neto R, Stavropoulos A, Schropp L, da Silveira HE, Wenzel A. Planning of dental implant size with digital panoramic radiographs, CBCT-generated panoramic images, and CBCT cross-sectional images. Clin Oral Implants Res. 2014;25:690–5. https://doi.org/10.1111/clr.12126.

56. Diniz AF, Mendonça EF, Leles CR, Guilherme AS, Cavalcante MP, Silva MA. Changes in the pre-surgical treatment planning using conventional spiral tomography. Clin Oral Implants Res. 2008;19:249–53. https://doi.org/10.1111/j.1600-0501.2007.01475.x.

57. Schropp L, Wenzel A, Kostopoulos L. Impact of conventional tomography on prediction of the appropriate implant size. Oral Surg Oral Med Oral Pathol Oral Radiol Endod. 2001;92:458–63. https://doi.org/10.1067/moe.2001.118286.

58. Schropp L, Stavropoulos A, Gotfredsen E, Wenzel A. Comparison of panoramic and conventional cross-sectional tomography for preoperative selection of implant size. Clin Oral Implants Res. 2011;22:424–9. https://doi.org/10.1111/j.1600-0501.2010.02006.x.

59. Baciut M, Hedesiu M, Bran S, Jacobs R, Nackaerts O, Baciut G. Pre- and postoperative assessment of sinus grafting procedures using cone-beam computed tomography compared with panoramic radiographs. Clin Oral Implants Res. 2013;24:512–6. https://doi.org/10.1111/j.1600-0501.2011.02408.x.

60. Lang AC, Schulze RK. Detection accuracy of maxillary sinus floor septa in panoramic radiographs using CBCT as gold standard: a multi-observer receiver operating characteristic (ROC) study. Clin Oral Investig. 2019;23:99–105. https://doi.org/10.1007/s00784-018-2414-1.

61. Pommer B, Ulm C, Lorenzoni M, Palmer R, Watzek G, Zechner W. Prevalence, location and morphology of maxillary sinus septa: systematic review and meta-analysis. J Clin Periodontol. 2012;39:769–73. https://doi.org/10.1111/j.1600-051X.2012.01897.x.

62. Fortin T, Camby E, Alik M, Isidori M, Bouchet H. Panoramic images versus three-dimensional planning software for oral implant planning in atrophied posterior maxillary: a clinical radiological study. Clin Implant Dent Relat Res. 2013;15:198–204. https://doi.org/10.1111/j.1708-8208.2011.00342.x.

63. Bertl K, Mick RB, Heimel P, Gahleitner A, Stavropoulos A, Ulm C. Variation in bucco-palatal maxillary sinus width does not permit a meaningful sinus classification. Clin Oral Implants Res. 2018;29:1220–9. https://doi.org/10.1111/clr.13387.

64. Chappuis V, Rahman L, Buser R, Janner SFM, Belser UC, Buser D. Effectiveness of contour augmentation with guided bone regeneration: 10-year results. J Dent Res. 2018;97:266–74. https://doi.org/10.1177/0022034517737755.

65. Fokas G, Vaughn VM, Scarfe WC, Bornstein MM. Accuracy of linear measurements on CBCT images related to presurgical implant treatment planning: a systematic review. Clin Oral Implants Res. 2018;29(Suppl 16):393–415. https://doi.org/10.1111/clr.13142.

66. Jung RE, Benic GI, Scherrer D, Hämmerle CH. Cone beam computed tomography evaluation of regenerated buccal bone 5 years after simultaneous implant placement and guided bone regeneration procedures—a randomized, controlled clinical trial. Clin Oral Implants Res. 2015;26:28–34. https://doi.org/10.1111/clr.12296.

67. Kaminaka A, Nakano T, Ono S, Kato T, Yatani H. Cone-beam computed tomography evaluation of horizontal and vertical dimensional changes in buccal Peri-implant alveolar bone and soft tissue: a 1-year prospective clinical study. Clin Implant Dent Relat Res. 2015;17(Suppl 2):e576–85. https://doi.org/10.1111/cid.12286.

68. Mengel R, Kruse B, Flores-de-Jacoby L. Digital volume tomography in the diagnosis of peri-implant defects: an in vitro study on native pig mandibles. J Periodontol. 2006;77:1234–41. https://doi.org/10.1902/jop.2006.050424.

69. Sbordone L, Toti P, Menchini-Fabris GB, Sbordone C, Piombino P, Guidetti F. Volume changes of autogenous bone grafts after alveolar ridge augmentation of atrophic maxillae and mandibles. Int J Oral Maxillofac Surg. 2009;38:1059–65. https://doi.org/10.1016/j.ijom.2009.06.024.

70. Schropp L, Wenzel A, Spin-Neto R, Stavropoulos A. Fate of the buccal bone at implants placed early, delayed, or late after tooth extraction analyzed by cone beam CT: 10-year results from a randomized, controlled, clinical study. Clin Oral Implants Res. 2015;26:492–500. https://doi.org/10.1111/clr.12424.

71. Smolka W, Eggensperger N, Carollo V, Ozdoba C, Iizuka T. Changes in the volume and density of calvarial split bone grafts after alveolar ridge augmentation. Clin Oral Implants Res. 2006;17:149–55. https://doi.org/10.1111/j.1600-0501.2005.01182.x.

72. Spin-Neto R, Stavropoulos A, Dias Pereira LA, Marcantonio E, Wenzel A. Fate of autologous and fresh-frozen allogeneic block bone grafts used for ridge augmentation. A CBCT-based analysis. Clin Oral Implants Res. 2013;24:167–73. https://doi.org/10.1111/j.1600-0501.2011.02324.x.

73. Corpas LS, Jacobs R, Quirynen M, Huang Y, Naert I, Duyck J. Peri-implant bone tissue assessment by comparing the outcome of intra-oral radiograph and cone beam computed tomography analyses to the histological standard. Clin Oral Implants Res. 2011;22:492–9. https://doi.org/10.1111/j.1600-0501.2010.02029.x.

74. Golubovic V, Mihatovic I, Becker J, Schwarz F. Accuracy of cone-beam computed tomography to assess the configuration and extent of ligature-induced peri-implantitis defects. A pilot study. Oral Maxillofac Surg. 2012;16:349–54. https://doi.org/10.1007/s10006-012-0320-2.

75. Ritter L, Elger MC, Rothamel D, et al. Accuracy of peri-implant bone evaluation using cone beam CT, digital intra-oral radiographs and histology. Dentomaxillofac Radiol. 2014;43:20130088. https://doi.org/10.1259/dmfr.20130088.

76. Wang D, Künzel A, Golubovic V, et al. Accuracy of peri-implant bone thickness and validity of assessing bone augmentation material using cone beam computed tomography. Clin Oral Investig. 2013;17:1601–9. https://doi.org/10.1007/s00784-012-0841-y.

77. Spin-Neto R, Marcantonio E, Gotfredsen E, Wenzel A. Exploring CBCT-based DICOM files. A systematic review on the properties of images used to evaluate maxillofacial bone grafts. J Digit Imaging. 2011;24:959–66. https://doi.org/10.1007/s10278-011-9377-y.

78. Schulze R, Heil U, Gross D, et al. Artefacts in CBCT: a review. Dentomaxillofac Radiol. 2011;40:265–73. https://doi.org/10.1259/dmfr/30642039.

79. Benic GI, Sancho-Puchades M, Jung RE, Deyhle H, Hämmerle CH. In vitro assessment of artifacts induced by titanium dental implants in cone beam computed tomography. Clin Oral Implants Res. 2013;24:378–83. https://doi.org/10.1111/clr.12048.

80. Bohner LOL, Tortamano P, Marotti J. Accuracy of linear measurements around dental implants by means of cone beam computed tomography with different exposure parameters. Dentomaxillofac Radiol. 2017;46:20160377. https://doi.org/10.1259/dmfr.20160377.

81. Gröbe A, Semmusch J, Schöllchen M, et al. Accuracy of bone measurements in the vicinity of titanium implants in CBCT data sets: a comparison of radiological and histological findings in Minipigs. Biomed Res Int. 2017;2017:3848207. https://doi.org/10.1155/2017/3848207.

82. Kamburoğlu K, Murat S, Kılıç C, et al. Accuracy of CBCT images in the assessment of buccal marginal alveolar peri-implant defects: effect of field of view. Dentomaxillofac Radiol. 2014;43:20130332. https://doi.org/10.1259/dmfr.20130332.

83. Liedke GS, Spin-Neto R, da Silveira HED, Schropp L, Stavropoulos A, Wenzel A. Factors affecting the possibility to detect buccal bone condition around dental implants using cone beam computed tomography. Clin Oral Implants Res. 2017;28:1082–8. https://doi.org/10.1111/clr.12921.

84. Liedke GS, Spin-Neto R, da Silveira HED, Schropp L, Stavropoulos A, Wenzel A. Accuracy of detecting and measuring buccal bone thickness adjacent to titanium dental implants-a cone beam computed tomography in vitro study. Oral Surg Oral Med Oral Pathol Oral Radiol. 2018;126:432–8. https://doi.org/10.1016/j.oooo.2018.06.004.

85. Raskó Z, Nagy L, Radnai M, Piffkó J, Baráth Z. Assessing the accuracy of cone-beam computerized tomography in measuring thinning Oral and buccal bone. J Oral Implantol. 2016;42:311–4. https://doi.org/10.1563/aaid-joi-D-15-00188.

86. Razavi T, Palmer RM, Davies J, Wilson R, Palmer PJ. Accuracy of measuring the cortical bone thickness adjacent to dental implants using cone beam computed tomography. Clin Oral Implants Res. 2010;21:718–25. https://doi.org/10.1111/j.1600-0501.2009.01905.x.

87. Domic D, Bertl K, Ahmad S, Schropp L, Hellén-Halme K, Stavropoulos A. Accuracy of cone-beam computed tomography is limited at implant sites with a thin buccal bone: a laboratory study. J Periodontol. 2021;92:592–601. https://doi.org/10.1002/JPER.20-0222.

88. Ferrus J, Cecchinato D, Pjetursson EB, Lang NP, Sanz M, Lindhe J. Factors influencing ridge alterations following immediate implant placement into extraction sockets. Clin Oral Implants Res. 2010;21:22–9. https://doi.org/10.1111/j.1600-0501.2009.01825.x.

89. Huynh-Ba G, Pjetursson BE, Sanz M, et al. Analysis of the socket bone wall dimensions in the upper maxilla in relation to immediate implant placement. Clin Oral Implants Res. 2010;21:37–42. https://doi.org/10.1111/j.1600-0501.2009.01870.x.

90. Pauwels R, Jacobs R, Singer SR, Mupparapu M. CBCT-based bone quality assessment: are Hounsfield units applicable. Dentomaxillofac Radiol. 2015;44:20140238. https://doi.org/10.1259/dmfr.20140238.

91. Turkyilmaz I, Ozan O, Yilmaz B, Ersoy AE. Determination of bone quality of 372 implant recipient sites using Hounsfield unit from computerized tomography: a clinical study. Clin Implant Dent Relat Res. 2008;10:238–44. https://doi.org/10.1111/j.1708-8208.2008.00085.x.

92. Nackaerts O, Maes F, Yan H, Couto Souza P, Pauwels R, Jacobs R. Analysis of intensity variability in multislice and cone beam computed tomogra-

phy. Clin Oral Implants Res. 2011;22:873–9. https://doi.org/10.1111/j.1600-0501.2010.02076.x.

93. Pauwels R, Nackaerts O, Bellaiche N, et al. Variability of dental cone beam CT grey values for density estimations. Br J Radiol. 2013;86:20120135. https://doi.org/10.1259/bjr.20120135.

94. Spin-Neto R, Gotfredsen E, Wenzel A. Variation in voxel value distribution and effect of time between exposures in six CBCT units. Dentomaxillofac Radiol. 2014;43:20130376. https://doi.org/10.1259/dmfr.20130376.

95. European Commission. Radiation protection no. 172. Evidence based guidelines based on cone beam CT for dental and maxillofacial radiology. Luxembourg: Office for Official Publications of the European Communities; 2012.

96. Marinescu Gava M, Suomalainen A, Vehmas T, Ventä I. Did malpractice claims for failed dental implants decrease after introduction of CBCT in Finland. Clin Oral Investig. 2019;23:399–404. https://doi.org/10.1007/s00784-018-2448-4.

97. Aiken A, Bouloux G, Hudgins P. MR imaging of the temporomandibular joint. Magn Reson Imaging Clin N Am. 2012;20:397–412. https://doi.org/10.1016/j.mric.2012.05.002.

98. Currie S, Hoggard N, Craven IJ, Hadjivassiliou M, Wilkinson ID. Understanding MRI: basic MR physics for physicians. Postgrad Med J. 2013;89:209–23. https://doi.org/10.1136/postgradmedj-2012-131342.

99. Gaudino C, Cosgarea R, Heiland S, et al. MR-imaging of teeth and periodontal apparatus: an experimental study comparing high-resolution MRI with MDCT and CBCT. Eur Radiol. 2011;21:2575–83. https://doi.org/10.1007/s00330-011-2209-0.

100. Kang Y, Hua C, Wu B, et al. Investigation of zero TE MR in preoperative planning in dentistry. Magn Reson Imaging. 2018;54:77–83. https://doi.org/10.1016/j.mri.2018.07.007.

101. Al-Haj Husain A, Valdec S, Stadlinger B, Rücker M, Piccirelli M, Winklhofer S. Preoperative visualization of the lingual nerve by 3D double-echo steady-state MRI in surgical third molar extraction treatment. Clin Oral Investig. 2022;26:2043–53. https://doi.org/10.1007/s00784-021-04185-z.

102. Assaf AT, Zrnc TA, Remus CC, et al. Evaluation of four different optimized magnetic-resonance-imaging sequences for visualization of dental and maxillo-mandibular structures at 3 T. J Craniomaxillofac Surg. 2014;42:1356–63. https://doi.org/10.1016/j.jcms.2014.03.026.

103. Burian E, Probst FA, Weidlich D, et al. MRI of the inferior alveolar nerve and lingual nerve-anatomical variation and morphometric benchmark values of nerve diameters in healthy subjects. Clin Oral Investig. 2020;24:2625–34. https://doi.org/10.1007/s00784-019-03120-7.

104. Hilgenfeld T, Kästel T, Heil A, et al. High-resolution dental magnetic resonance imaging for planning palatal graft surgery-a clinical pilot study.

J Clin Periodontol. 2018;45:462–70. https://doi.org/10.1111/jcpe.12870.

105. de Carvalho E, Silva Fuglsig JM, Wenzel A, Hansen B, Lund TE, Spin-Neto R. Magnetic resonance imaging for the planning, execution, and follow-up of implant-based oral rehabilitation: systematic review. Int J Oral Maxillofac Implants. 2021;36:432–41. https://doi.org/10.11607/jomi.8536.

106. Grandoch A, Peterke N, Hokamp NG, Zöller JE, Lichenstein T, Neugebauer J. 1.5 T MRI with a dedicated dental signal-amplification coil as noninvasive, radiation-free alternative to CBCT in presurgical implant planning procedures. Int J Oral Maxillofac Implants. 2021;36:1211–8. https://doi.org/10.11607/jomi.8103.

107. Flügge T, Ludwig U, Hövener JB, Kohal R, Wismeijer D, Nelson K. Virtual implant planning and fully guided implant surgery using magnetic resonance imaging-proof of principle. Clin Oral Implants Res. 2020;31:575–83. https://doi.org/10.1111/clr.13592.

108. Flügge T, Ludwig U, Winter G, Amrein P, Kernen F, Nelson K. Fully guided implant surgery using magnetic resonance imaging—an in vitro study on accuracy in human mandibles. Clin Oral Implants Res. 2020;31:737–46. https://doi.org/10.1111/clr.13622.

109. Hilgenfeld T, Juerchott A, Deisenhofer UK, et al. In vivo accuracy of tooth surface reconstruction based on CBCT and dental MRI-A clinical pilot study. Clin Oral Implants Res. 2019;30:920–7. https://doi.org/10.1111/clr.13498.

110. Erasmus LJ, Hurter D, Naudé M, Kritzinger HG, Acho S. A short overview of MRI artefacts. S Afr J Radiol. 2004;8:13.

111. Gao X, Wan Q, Gao Q. Susceptibility artifacts induced by crowns of different materials with prepared teeth and titanium implants in magnetic resonance imaging. Sci Rep. 2022;12:428. https://doi.org/10.1038/s41598-021-03962-w.

112. Hilgenfeld T, Prager M, Schwindling FS, et al. Artefacts of implant-supported single crowns—impact of material composition on artefact volume on dental MRI. Eur J Oral Implantol. 2016;9:301–8.

113. Demirturk Kocasarac H, Ustaoglu G, Bayrak S, et al. Evaluation of artifacts generated by titanium, zirconium, and titanium-zirconium alloy dental implants on MRI, CT, and CBCT images: a phantom study. Oral Surg Oral Med Oral Pathol Oral Radiol. 2019;127:535–44. https://doi.org/10.1016/j.oooo.2019.01.074.

114. Bohner L, Meier N, Gremse F, Tortamano P, Kleinheinz J, Hanisch M. Magnetic resonance imaging artifacts produced by dental implants with different geometries. Dentomaxillofac Radiol. 2020;49:20200121. https://doi.org/10.1259/dmfr.20200121.

115. Duttenhoefer F, Mertens ME, Vizkelety J, Gremse F, Stadelmann VA, Sauerbier S. Magnetic resonance imaging in zirconia-based dental implantology. Clin Oral Implants Res. 2015;26:1195–202. https://doi.org/10.1111/clr.12430.

116. Smeets R, Schöllchen M, Gauer T, et al. Artefacts in multimodal imaging of titanium, zirconium and binary titanium-zirconium alloy dental implants: an in vitro study. Dentomaxillofac Radiol. 2017;46:20160267. https://doi.org/10.1259/dmfr.20160267.

117. Hilgenfeld T, Juerchott A, Deisenhofer UK, et al. Accuracy of cone-beam computed tomography, dental magnetic resonance imaging, and intraoral radiography for detecting peri-implant bone defects at single zirconia implants-an in vitro study. Clin Oral Implants Res. 2018;29:922–30. https://doi.org/10.1111/clr.13348.

118. Wanner L, Ludwig U, Hövener JB, Nelson K, Flügge T. Magnetic resonance imaging-a diagnostic tool for postoperative evaluation of dental implants: a case report. Oral Surg Oral Med Oral Pathol Oral Radiol. 2018;125:e103–7. https://doi.org/10.1016/j.oooo.2018.01.005.

119. Senel FC, Duran S, Icten O, Izbudak I, Cizmeci F. Assessment of the sinus lift operation by magnetic resonance imaging. Br J Oral Maxillofac Surg. 2006;44:511–4. https://doi.org/10.1016/j.bjoms.2006.02.004.

120. Flügge T, Ludwig U, Amrein P, et al. MRI for the display of autologous onlay bone grafts during early healing-an experimental study. Dentomaxillofac Radiol. 2021;50:20200068. https://doi.org/10.1259/dmfr.20200068.

121. Schropp L, Wenzel A, Kostopoulos L, Karring T. Bone healing and soft tissue contour changes following single-tooth extraction: a clinical and radiographic 12-month prospective study. Int J Periodontics Restorative Dent. 2003;23:313–23.

122. Brägger U, Bürgin W, Lang NP, Buser D. Digital subtraction radiography for the assessment of changes in peri-implant bone density. Int J Oral Maxillofac Implants. 1991;6:160–6.

123. Jeffcoat MK. Digital radiology for implant treatment planning and evaluation. Dentomaxillofac Radiol. 1992;21:203–7. https://doi.org/10.1259/dmfr.21.4.1299635.

124. Jeffcoat MK, Reddy MS, van den Berg HR, Bertens E. Quantitative digital subtraction radiography for the assessment of peri-implant bone change. Clin Oral Implants Res. 1992;3:22–7.

125. Reddy MS, Jeffcoat MK, Richardson RC. Assessment of adjunctive flurbiprofen therapy in root-form implant healing with digital subtraction radiography. J Oral Implantol. 1990;16:272–6.

126. Reddy MS, Mayfield-Donahoo TL, Jeffcoat MK. A semi-automated computer-assisted method for measuring bone loss adjacent to dental implants. Clin Oral Implants Res. 1992;3:28–31.

127. Garetto LP, Chen J, Parr JA, Roberts WE. Remodeling dynamics of bone supporting rigidly fixed titanium implants: a histomorphometric comparison in four species including humans. Implant Dent. 1995;4:235–43.

128. Gotfredsen K, Budtz-Jörgensen E, Jensen LN. A method for preparing and staining histological sections containing titanium implants for light microscopy. Stain Technol. 1989;64:121–7.

129. Sennerby L, Ericson LE, Thomsen P, Lekholm U, Astrand P. Structure of the bone-titanium interface in retrieved clinical oral implants. Clin Oral Implants Res. 1991;2:103–11.

130. Cattaneo PM, Dalstra M, Melsen B. The finite element method: a tool to study orthodontic tooth movement. J Dent Res. 2005;84:428–33. https://doi.org/10.1177/154405910508400506.

131. Dalstra M, Cattaneo PM, Beckmann F. Synchrotron radiation-based microtomography of alveolar support tissues. Orthod Craniofac Res. 2006;9:199–205. https://doi.org/10.1111/j.1601-6343.2006.00376.x.

132. Bouxsein ML, Boyd SK, Christiansen BA, Guldberg RE, Jepsen KJ, Müller R. Guidelines for assessment of bone microstructure in rodents using micro-computed tomography. J Bone Miner Res. 2010;25:1468–86. https://doi.org/10.1002/jbmr.141.

133. Elliott JC, Dover SD. X-ray microtomography. J Microsc. 1982;126:211–3.

134. Feldkamp LA, Goldstein SA, Parfitt AM, Jesion G, Kleerekoper M. The direct examination of three-dimensional bone architecture in vitro by computed tomography. J Bone Miner Res. 1989;4:3–11. https://doi.org/10.1002/jbmr.5650040103.

135. Layton MW, Goldstein SA, Goulet RW, Feldkamp LA, Kubinski DJ, Bole GG. Examination of subchondral bone architecture in experimental osteoarthritis by microscopic computed axial tomography. Arthritis Rheum. 1988;31:1400–5.

136. Odgaard A. Three-dimensional methods for quantification of cancellous bone architecture. Bone. 1997;20:315–28.

137. Kiba H, Hayakawa T, Oba S, Kuwabara M, Habata I, Yamamoto H. Potential application of high-resolution microfocus X-ray techniques for observation of bone structure and bone-implant interface. Int J Oral Maxillofac Implants. 2003;18:279–85.

138. Sennerby L, Wennerberg A, Pasop F. A new microtomographic technique for non-invasive evaluation of the bone structure around implants. Clin Oral Implants Res. 2001;12:91–4.

139. Van Oossterwyck H, Duyck J, Vander Sloten J, et al. Use of microfocus computerized tomography as a new technique for characterizing bone tissue around oral implants. J Oral Implantol. 2000;26:5–12. https://doi.org/10.1563/1548-1336(2000)026<0005:TUOMCT>2.3.CO;2.

140. Yip G, Schneider P, Roberts EW. Micro-computed tomography: high resolution imaging of bone and implants in three dimensions. Semin Orthod. 2004;10:174–87.

141. Vandeweghe S, Coelho PG, Vanhove C, Wennerberg A, Jimbo R. Utilizing micro-computed tomography to evaluate bone structure surrounding dental implants: a comparison with histomorphometry. J Biomed

Mater Res B Appl Biomater. 2013;101:1259–66. https://doi.org/10.1002/jbm.b.32938.

142. Schouten C, Meijer GJ, van den Beucken JJ, Spauwen PH, Jansen JA. The quantitative assessment of peri-implant bone responses using histomorphometry and micro-computed tomography. Biomaterials. 2009;30:4539–49. https://doi.org/10.1016/j.biomaterials.2009.05.017.

143. Stoppie N, van der Waerden JP, Jansen JA, Duyck J, Wevers M, Naert IE. Validation of microfocus computed tomography in the evaluation of bone implant specimens. Clin Implant Dent Relat Res. 2005;7:87–94.

144. Neldam CA, Pinholt EM. Synchrotron μCT imaging of bone, titanium implants and bone substitutes - a systematic review of the literature. J Craniomaxillofac Surg. 2014;42:801–5. https://doi.org/10.1016/j.jcms.2013.11.015.

145. Neldam CA, Sporring J, Rack A, et al. Synchrotron radiation μCT and histology evaluation of bone-to-implant contact. J Craniomaxillofac Surg. 2017;45:1448–57. https://doi.org/10.1016/j.jcms.2017.05.019.

146. Arvidsson A, Sarve H, Johansson CB. Comparing and visualizing titanium implant integration in rat bone using 2D and 3D techniques. J Biomed Mater Res B Appl Biomater. 2015;103:12–20. https://doi.org/10.1002/jbm.b.33168.